Reprinted from The Journal of Physical Chemistry, 1993, 97.

Molecular Dynamics Simulation of a Bilayer of 200 Lipids in the Gel and in the Liquid-Crystal Phases

Helmut Heller,† Michael Schaefer,‡ and Klaus Schulten*

Beckman Institute and Department of Physics, University of Illinois, 405 North Mathews Avenue, Urbana, Illinois 61801

Received: December 21, 1992; In Final Form: February 23, 1993

We have constructed and simulated a membrane–water system which consists of 200 molecules of 1-palmitoyl-2-oleoyl-*sn*-glycero-3-phosphatidylcholine forming a rectangular patch of a bilayer and of 5483 water molecules covering the head groups on each side of the bilayer. The total number of atoms is approximately 27 000. The lateral dimensions of the bilayer are 85 Å × 100 Å, and the distance between the bilayer surfaces as given by the average phosphorus to phosphorus distance is 35 Å. The thickness of each water layer is up to 15 Å. In all, we simulated 263 ps of the dynamics of the system. To prevent system disintegration, atoms within 5 Å from the surface were harmonically restrained and treated by Langevin dynamics, forming a stochastic boundary. Interior lipids and water molecules were unrestrained. The first 120 ps of the dynamics calculation were used to equilibrate the system and to achieve a low internal pressure. We performed two simulations for analysis: simulation I of the system that resulted from the equilibration; simulation II of the system after an increase of the area per head group from 46 to 70 Å^2. The decrease of the lateral lipid density was achieved by scaling the atomic x-, y-, and z-coordinates independently, leaving the volume of the system constant. For both simulations I and II, we determined the internal pressure, the lipid self-diffusion coefficients, the order parameter profile, the distribution of molecular groups, and other properties. The parameters extracted from simulation II are in good agreement with observations on bilayers in the liquid-crystal phase. We provide evidence that the bilayer of simulation I corresponds to the gel phase. The membrane structures resulting from this work can be used for molecular dynamics investigations of membrane proteins, e.g., for the study of lipid–protein interactions or for the equilibration of structural models.

Membrane proteins and membrane related processes have been the subject of experimental[2-5] and theoretical[6-11] research during the past 40 years. The interest of the theoretical community in investigating biological membranes has been relatively low. One reason may have been the fact that only very little structural information on membranes and on membrane proteins exists. Another reason might be the statistical nature of lipid membrane structures which requires either large systems and/or long time ranges for proper characterizations. Also, because of limitations in computer power, researchers until recently were generally restricted to molecular dynamics studies of biopolymer systems entailing only a few thousands atoms,[12-15] which is too few to encompass membranes and membrane–protein systems. There is evidence, however, that the environment has a strong influence on the structure and function of proteins, both in solution and in membranes,[11,16-19] and, hence, a study of membranes with and without proteins is most desirable.

Early theoretical investigations of membranes were carried out by Marčelja,[6] who introduced a molecular field model to represent the influence of neighboring lipid molecules. One drawback of this approach is that it cannot reproduce cooperative effects of several lipid molecules. As computers became more powerful, molecular dynamics (MD) simulations of small lipid systems (2 × 16 decanoate molecules) over short times of the order of 100 ps became feasible.[20] Periodic boundary conditions together with the small system size gave rise to artifacts which were reduced in later studies by increasing the system size to 2 × 64 decane molecules.[21] Simulation of *complete* lipid molecules (2 × 24 1,2-dimyristoyl-*sn*-glycero-3-phosphatidylethanolamine (DMPE) molecules and 553 water molecules[22]) made the model more realistic. Another improvement was the inclusion of water and ions in the simulation.[23] In addition to monolayers and bilayers, micelle–water systems have also been simulated.[24,25]

The time range of the simulations listed above is of the order of 100 ps. Such a short time range prevents the investigation of many membrane properties, e.g., of phase transitions, which occur on time scales in the range of microseconds and longer. A combination of Brownian dynamics with the Marčelja molecular field model allowed the simulation of a single chain of a DPPC molecule for 0.66 μs.[26,27] Here too, the simulations were improved by increasing the size of the system to as much as 84 molecules.[10,28]

One very promising outcome of simulations of biological membranes is use of the simulated systems in investigations of membrane–protein interactions.[16] With the advent of modern supercomputers, especially of parallel machines providing computing power in the giga floating point operations per second (GFLOPS) range,[29,30] and with the development of efficient algorithms for the evaluation of long-range Coulomb forces,[1,31-35] the study of large and heterogeneous systems using molecular dynamics has become increasingly feasible. In this article, we report on molecular dynamics simulations on a self-built parallel computer[29] of a 85 Å × 100 Å patch of membrane bilayer covered with up to 15 Å of water on each side. The system was specifically chosen large enough to accommodate a membrane protein of about 20 000 molecular weight, e.g., bacteriorhodopsin, and for the purpose of embedding larger proteins it can easily be enlarged. Another objective of this work was to ensure that the simulated bilayer is in the liquid-crystal phase (L_α) which is the biologically most relevant membrane phase.[36] From experiments, it is known that 1-palmitoyl-2-oleoyl-*sn*-glycero-3-phosphatidylcholine (POPC) is in the liquid-crystal phase in a wide temperature range from −5 to +70 °C.[37] Other important membrane phases are the crystal phase (L_c) and the gel phase ($L_{\beta'}$).[38]

In the following section, we describe the construction of a

* To whom correspondence should be addressed.
† Present address: Institute for Medical Optics, Ludwig Maximilians University, Theresienstrasse 37, 80333 Munich, Germany (e-mail: heller@lisboa.ks.uiuc.edu).
‡ Present address: Department of Chemistry, Harvard University, 12 Oxford St., Cambridge, MA 02138.

0022-3654/93/2097-8343$04.00/0

starting configuration of the bilayer and the methods used for simulating the system, for changing the system setup, and for analyzing the trajectories. In the Results section, we report on five molecular dynamics calculations, termed Equilibration, Simulation I, "Disaster I" and "Disaster II", and Simulation II. During equilibration, special emphasis was put on investigating and adjusting the pressure in the system which involved a series of changes of the stochastic boundary setup. The simulation conditions were invariant during simulations I and II which were calculated for detailed analysis. The initial structure of simulation II was generated from the final structure of simulation I by increasing the lateral area of the bilayer by 50%. The simulations "Disaster I" and "Disaster II" are two unsuccessful attempts at inducing such an increase. The alteration in the simulation conditions in going from simulation I to simulation II successfully induced a phase change in the bilayer from the gel phase ($L_{\beta'}$) to the liquid-crystal phase (L_α).

Methods

Parallel Computation. For the molecular dynamics simulations reported in this article, we employed a 60 node multiple instructions, multiple data (MIMD) type parallel computer with double ring architecture which was built in our research group.[29,39] Each node of this machine consists of a T800 Transputer processor with 4 Mbyte dynamic random access memory (DRAM). The computer achieves Cray 2 processor speed for molecular dynamics calculations.[40,41] The total computer time for all the simulations described in this paper amounts to more than 14 640 h or 20 months of continuous run time.

We used the molecular dynamics program EGO.[29,41-43] EGO is written in OCCAM II and achieves a speed proportional to the number of nodes. The program is input/output compatible with CHARMm[44] and X-PLOR.[45,46] EGO employs the CHARMm force field and can be started using X-PLOR restart files. The program uses a modified Verlet algorithm[47] with a distance class algorithm[1] for the nonbonded interactions; i.e., it does not truncate the Coulomb and van der Waals forces (a paper which focuses on the consequences of cutoff in membrane simulations is currently in preparation). With respect to the electrostatic interaction, the distance class algorithm is an alternative to the fast multipole algorithm.[33] A parallel version of the SHAKE algorithm[48,49] constrains the bond length for hydrogen atoms and allows an integration time step of 1 fs. For the analysis of the simulation data, we used X-PLOR[46] as well as software developed by the authors.

Construction of the Membrane Bilayer. We chose POPC as the lipid for the construction of the bilayer, because it is one of the most prevailing phospholipids. POPC has one saturated palmitoyl and one unsaturated oleoyl fatty acid tail. The presence of one unsaturated hydrocarbon tail enables one to study effects of unsaturation. The lipid can be easily altered to DPPC, probably the most widely studied phospholipid.

We constructed one POPC molecule using the program *ChemNote* within the molecular graphics package *Quanta*.[50] Hydrogen atoms were represented by compound atoms. The chemical structure of POPC is given in Figure 1. In the initial structure of this molecule all dihedrals of the tails and head group were in the *trans* form, except for the C=C double bond which was in the *cis* form.

With interactive graphics, we arranged the lipid in an extended "upright" configuration, with both hydrocarbon tails and the head group pointing along the y-axis, which was to become the bilayer normal. After 100 steps of steepest descent minimization within *Quanta*, four identical copies of the molecule were arranged in a staggered configuration, forming the building block for the monolayer (see Figure 2). After another minimization of 200 steps, we calculated a 1-ps molecular dynamics trajectory applying velocity rescaling in order to reduce the energy content of the

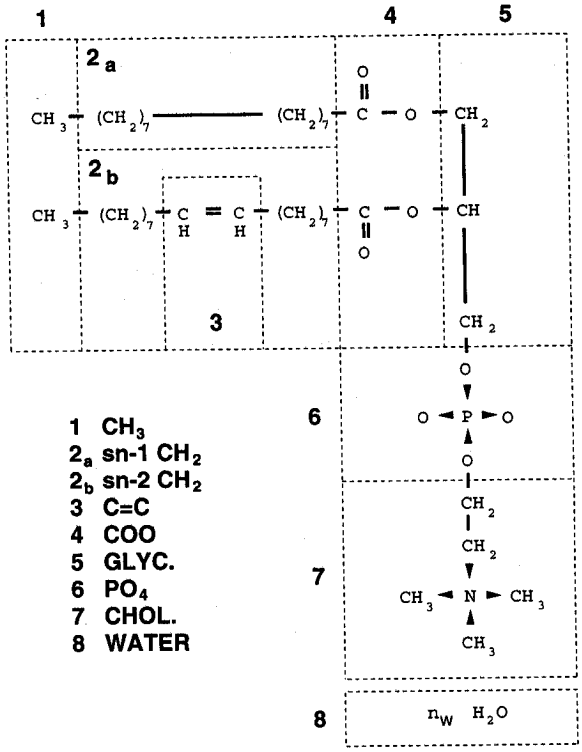

Figure 1. Chemical structure of POPC and the classification of lipid and water atoms into eight groups. The classification refers to the cross-membrane profiles, below, and is analogous to the parsing of DOPC in ref 51.

building block. At first, the system spontaneously heated up to a temperature of 600 K, but, within the simulation time of 1 ps, it reached the target temperature of 300 K. The preparation of the building block was then completed by another 100 steps of steepest descent minimization. Subsequently, 25 building blocks were arranged in a 5 × 5 grid to form one layer of the membrane, which was minimized for 100 steps. This layer was duplicated, rotated, and shifted to obtain a bilayer, leaving a 1-Å distance between the maximum y-coordinate of atoms in the lower layer and the minimum y-coordinate of atoms in the upper layer. We obtained a membrane patch with a lateral area of 68 Å × 80 Å and a thickness of 44 Å, the latter referring to the average phosphorus to phosphorus distance between the monolayers.

To complete the construction, the two membrane surfaces were covered by up to 15 Å of water (see Figure 3) which corresponds to approximately six layers of water molecules. Additional water molecules were placed in the head group region to fill available space. The initial positions of the water oxygen atoms were on a hexagonal lattice with a unit cell size corresponding to the density of water at normal conditions. The orientation of the hexagonal lattice as well as the orientation of each water molecule was chosen at random. The resulting initial system consisted of 200 lipid molecules and 4526 water molecules with the total number of atoms equal to 23 978.

To equilibrate the system, we computed a trajectory of more than 120 ps. For the lipid molecules, we used the atom type assignments and the partial charge set provided by *ChemNote* within *Quanta*. The bonded and van der Waals potential parameters were taken from the parameter file param19.pro of X-PLOR. For the water molecules we employed TIPS3P (parameter file param19.sol of X-PLOR) parameters.[52] After the equilibration, we adopted a data set (parameter and topology file Charmm22 of CHARMm) provided to us by A. MacKerell of the Department of Chemistry at Harvard[53] for the lipid partial charges. The parameters of the bonded potential and of the van der Waals potential were not changed.

At the beginning of simulation II, we changed the lateral area per lipid molecule to achieve agreement with experimental data

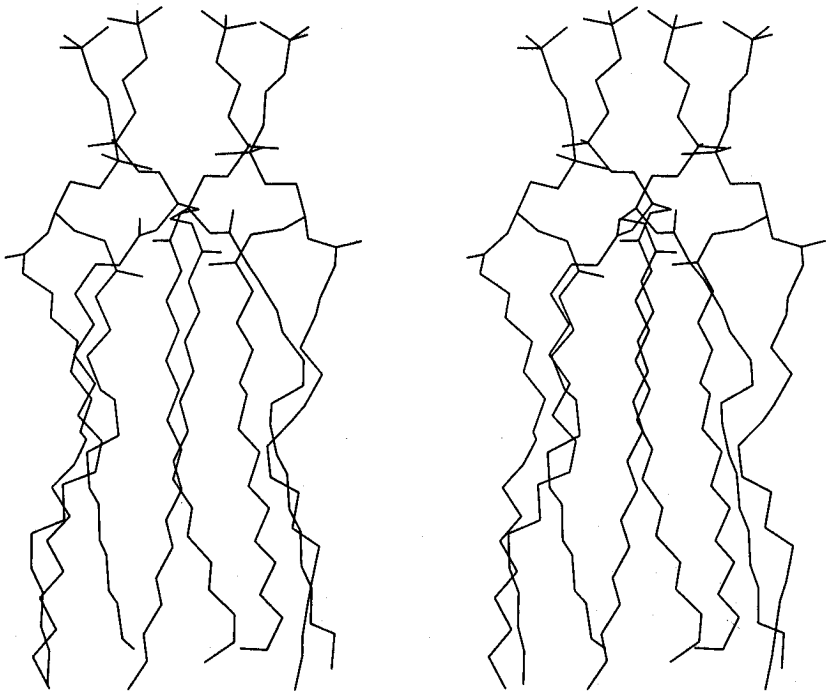

Figure 2. Stereo diagram of the building block of four lipids ((left) left eye view; (right) right eye view). The lipids are arranged in a staggered configuration such that the tail of one lipid reaches into the void between the two tails of another lipid.

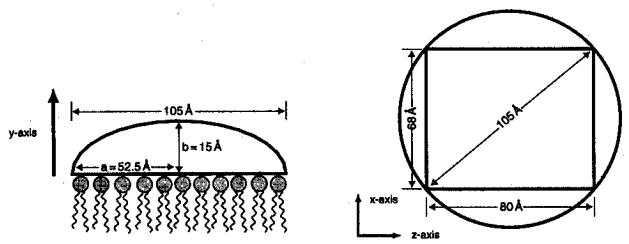

Figure 3. Schematic diagram of one water cap in the initial membrane geometry used during equilibration, simulation I, disaster I, and disaster II. For each water molecule, the distance d from the bilayer surface satisfies $d(x,z) \leq [b^2 - b^2(x^2 + z^2)/a^2]^{1/2}$, where $2a$ is the diagonal of the bilayer surface, $b = 15$ Å the maximum thickness of the water cap, and x, y, z are the coordinates of the water molecule, with the bilayer centered at the origin. The water molecules are therefore located inside an ellipsoid generated by rotation around the bilayer normal. Left: side view of the upper water cap with one diagonal of the bilayer surface in the paper plane. Right: top view; no water molecules were placed outside the rectangular membrane surface.

(see the section on coordinate rescaling) and we constructed new water caps. For simplicity, these water caps were given a rectangular geometry and the water oxygen atoms were placed initially on a cubic lattice. As with the original water caps, the orientation of the water molecules and of the whole lattice was chosen at random. The thickness of the two water layers was 10 Å which, in conjunction with the increased lateral dimensions of the bilayer of 85 Å × 100 Å, led to a total number of 5483 water molecules. Accordingly, the total number of atoms of the bilayer–water system increased to 26 849.

Stochastic Boundary. A stochastic boundary (Langevin dynamics)[54,55] with harmonic restraints was used to couple the system to a heat bath and prevent system disintegration. The Langevin dynamics algorithm implemented by EGO is as described in ref 56, and the harmonic restraint energy of an atom is calculated according to $E_{har} = k_{har}(\vec{P} - \vec{P}_0)^2$, where $\vec{P}$ and $\vec{P}_0$ are the location of the atom and its reference position. During all simulations reported in this paper, the heat bath temperature, affecting atoms in the stochastic boundary only, was set equal to 300 K.

Friction and stochastic forces were gradually increased from the inside to the outside within a boundary of thickness $\Delta = 8$ Å. During simulation II, the boundary thickness was reduced to $\Delta = 5$ Å. For an atom at position $\vec{P}$, a switching function $S(\vec{P})$ was used to determine the harmonic force constant of the restraining potential $k_{har}(\vec{P}) = k_{max}S(\vec{P})$, and the collision frequency $f(\vec{P}) = f_{max}S(\vec{P})$. For simplicity, we used an atom-type independent maximum collision frequency of $f_{max} = 30$/ps and a maximum harmonic force constant of $k_{max} = 17.2$ kcal/(mol Å^2), which corresponds to a harmonic oscillation frequency of $\omega = 20$/ps. Hydrogens were not assigned friction or harmonic force constants. The switching function $S(\vec{P})$ is a combination of two switching parameters, one depending on the minimum distance d_{xz} to the lateral boundary and the other depending on the minimum distance d_y to the surface of the water caps

$$S(\vec{P}) = F_s(\Delta - d_{xz}) + F_s(\Delta - d_y) - [F_s(\Delta - d_{xz})\,F_s(\Delta - d_y)]^{1/2} \quad (1)$$

Here, F_s is the switching function

$$F_s(x) = \begin{cases} 0, & \text{if } x \leq 0 \\ x^2(3\Delta - 2x)/(2\Delta^3), & \text{if } 0 \leq x \leq \Delta \\ 1/2, & \text{if } x \geq \Delta \end{cases} \quad (2)$$

During simulation I, the harmonic restraints on lipid atoms were reduced by a factor of 50 and those on water oxygens by a factor of 5 in order to reduce the rigidity of the boundary. During simulation II, only the lipid phosphorus atoms and water oxygens were restrained and the maximum harmonic force constant was reduced by a factor of 5. The maximum friction constant was kept at the value given above.

Pressure and Surface Tension. The pressure in the system was determined in two different ways: by evaluating the forces on the boundary atoms from the harmonic restraints (boundary method) and by using the virial method.[57] Because EGO does not provide easy access to the forces and velocities during a dynamics run, we used the virial method only in a few instances to check the pressures which were obtained with the boundary method.

Surface Tension. Since the dimensions of the system described here are very small compared to macroscopic systems, the contributions of the surface tension to the pressure cannot be neglected. Assuming a spherical system with radius R, this contribution is $p_{surf} = -2\sigma/R$, where σ is the surface tension. The

negative sign of the pressure reflects the tendency of the surface tension to reduce the size of the system. From the volume of the membrane–water system, one can estimate $R \approx 36.5$ Å, while the surface tension at the interface between water and air at 305 K is $\sigma = 0.071$ N/m.[58,59] We, therefore, have an approximate contribution of $p_{surf} \approx -39$ MPa to the pressure in the system (1 MPa = 10^6N/m^2 = 10 bar). These considerations apply to both equilibration and simulation I, for which we had chosen a curved outer boundary for the two water caps, with a radius of curvature in the range from 15 to about 60 Å. For a rectangular system, one can derive an expression for the pressure contribution from surface tension that is identical to the one above, with R now the thickness of the bilayer.[21] The difference is that, for this geometry, the contribution is to the lateral pressure only.

Boundary Method. The pressures on the six faces of the system were calculated independently. Ignoring the curvature of the two surfaces in the y-direction, the total surface is given by six rectangles. To reduce the risk of introducing an error in the pressure calculation related to the edges and corners of the system boundary, we cut off 15 Å from the edges of each surface rectangle. $\hat{n}$ is given as the normal vector on a surface rectangle, pointing outward. To calculate the pressure on the surface rectangle, we determined the boundary atoms belonging to it, calculated the negative sum of all restraining forces acting on them, took the scalar product of that force with $\hat{n}$, and divided by the area A of the rectangle:

$$p(t) = -\frac{1}{A}\sum_i \vec{F}_i^{\,har}(t)\hat{n} \tag{3}$$

$$\vec{F}_i^{\,har}(t) = -2k_i^{har}(\vec{P}_i(t) - \vec{P}_i(0)) \tag{4}$$

Here, k_i^{har} is the force constant of the restraining potential (see the section on the stochastic boundary) and $\vec{P}_i(t)$ the actual and $\vec{P}_i(0)$ the reference position of atom i. Note that a shift of atom i toward the outside, i.e., $(\vec{P}_i(t) - \vec{P}_i(0))\cdot\hat{n} > 0$, leads to a positive pressure contribution even though the restraining force points inward.

Virial Method. According to the virial method,[57] the pressure of a molecular system is given by

$$p = \frac{2}{3V}(E_{kin} - \Xi) \tag{5}$$

where Ξ is the internal virial for pair-additive potentials, E_{kin} is the kinetic energy, and V is the volume of the system. Because intramolecular forces necessarily sum up to zero, the internal virial Ξ is given by

$$\Xi = -\frac{1}{2}\sum_{i<j}(\vec{P}_i^{CM} - \vec{P}_j^{CM})\cdot\vec{F}_{ij} \tag{6}$$

where $\vec{P}_i^{CM}$ is the location of the center of mass of molecule i and $\vec{F}_{ij}$ is the net force exerted by molecule j on molecule i. Note that only van der Waals and Coulomb interactions contribute to $\vec{F}_{ij}$.

Rescaling of Coordinates and Reference Positions. At various points in our simulation it was necessary to change the size of the system. For this purpose we employed two different schemes, termed atomic rescaling and molecular rescaling. Atomic rescaling was done by multiplying all coordinates by a scaling factor f. We generalized this method by allowing for an independent rescaling of the atomic x-, y-, and z-coordinates with scaling factors f_x, f_y, and f_z, respectively. This non-uniform scaling procedure enabled us to change the shape of the membrane patch, e.g., to reduce the thickness of the bilayer without altering the lateral area. In order to make small adjustments or to shrink the system, we rescaled only the reference positions for the harmonic restraints. When continuing the molecular dynamics simulation, this change would affect only atoms in the boundary which were assigned a non-zero restraining force constant. Due to the harmonic restraint forces, the simulated system gradually adjusted to the altered boundary.

At the beginning of simulation II, we increased the area per head group by a factor of 1.5 compared to the equilibration or simulation I. Such a drastic change could not be accomplished by rescaling of the reference positions, since this caused extremely high restraint energies of the order of 10^5 kcal/mol and very high temperatures during the simulation (see "Disaster II"). Therefore, we changed both the reference positions and the actual coordinates of the atoms.

However, atomic rescaling of the positions inevitably distorts the molecular structure, in particular bond lengths, and, if non-uniform scaling is used, also bond angles and dihedrals. A rescaling by a factor as large as 1.5 would introduce large, unwanted contributions into the bonded energy and force terms. Therefore, we adopted a method which we termed molecular rescaling. First, the centers of mass $\vec{P}_i^{CM}$ of all molecules were determined. Every molecule was then shifted as a whole, with the shift vector $\vec{s}_i$ of molecule i being calculated according to $\vec{s}_i = (f - 1)\,\vec{P}_i^{CM}$. Therefore, the new coordinates of an atom belonging to molecule i were given by $\vec{P}_{new} = \vec{P}_{old} + \vec{s}_i$. This procedure was only suitable for an expansion of the system ($f > 1$) since, in the case of a contraction, the van der Waals repulsion of close contacts would induce very strong forces. As in the case of the atomic rescaling procedure, we scaled the scaling x-, y-, and z-coordinates independently.

Distribution of Molecular Groups. To determine the distribution of molecular groups across the membrane, i.e., along the y-axis, we used an area $A_{xz}(y)$ parallel to the bilayer surface for sampling. To define the dimensions of A_{xz}, we started with the smallest rectangle covering all atomic positions of the membrane patch projected onto the xz plane and then cut off 15 Å from all four sides, thus avoiding sampling over restrained atoms in the lateral boundary. The following procedure allowed us to deduce continuous profiles from our data despite the relatively small number of atoms or molecules involved. First, we assigned to the quantities under consideration, e.g., to all CH_2 units, normalized, three dimensional Gaussian density functions:

$$G_i(\vec{x}) = \frac{1}{\pi^{3/2}\sigma^3}\exp(-(\vec{x} - \vec{x}_i)^2/\sigma^2) \tag{7}$$

Here, $\vec{x}_i$ denotes the location of unit i. We typically used a value $\sigma = 1.5$ Å for the width to ensure atomic resolution. The average density $\rho(y)$ as a function of y was then determined by integrating the sum of the density functions G_i over $A_{xz}(y)$ and dividing by the area of A_{xz}:

$$\rho(y) = \frac{1}{|A_{xz}|}\sum_i \int_{A_{xz}(y)} G_i\, d^3x \tag{8}$$

In this expression, the area of A_{xz} is denoted by $|A_{xz}|$. If A_{xz} extends from $-a$ to $+a$ in the x-direction and from $-b$ to $+b$ in the z-direction, the contribution of a single unit i at (x_i,y_i,z_i) is

$$\int_{A_{xz}(y)} G_i\, d^3x = \frac{1}{4\pi^{1/2}\sigma}\exp\left(-\frac{(y_i - y)^2}{\sigma^2}\right)\left[\mathrm{erf}\left(\frac{a + x_i}{\sigma}\right) + \mathrm{erf}\left(\frac{a - x_i}{\sigma}\right)\right]\left[\mathrm{erf}\left(\frac{b + z_i}{\sigma}\right) + \mathrm{erf}\left(\frac{b - z_i}{\sigma}\right)\right] \tag{9}$$

where erf(z) denotes the error function.

For averaging distributions calculated at different times along a trajectory, it was necessary to define a zero point of the y-axis which is insensitive to a translation of the whole system. This was accomplished by shifting the geometric center of the lipids to the origin prior to calculating a distribution. The geometric center was determined by averaging the x-, y-, and z-coordinates of all lipid atoms in the system.

Area per Head Group. To calculate the average area per lipid head group, we first determined the area A_{xz} of the smallest rectangle covering the lipid atoms projected onto the xz plane. The area per lipid is then given by simply dividing A_{xz} by the number of lipid molecules in one layer, namely, by 100. To improve the accuracy, we used a set of 20 rectangles for sampling and averaging. The first sampling area was generated by cutting 10 Å off the edges of the lateral covering area referred to above. All rectangles had the origin as center, and their length in the x-direction and in the z-direction was decreased by 1 Å in going from one rectangle to the next. For each rectangle and for both the upper and the lower layer of the membrane, we determined the number of lipid molecules, represented by their center of mass, within the sampling area and then divided the rectangle area by that number. This procedure provided us with a set of 40 values for the area per head group from which we determined both the average area and the standard deviation.

^{2}H Order Parameter. The deuterium order parameter S_{CD} is a critical source of structural and dynamical information on lipids. It is related to the average orientation of the methylene groups and provides information about the order within the bilayer. The traceless order parameter tensor S is defined as

$$S_{ij} = {}^1/_2\langle 3 \cos\theta_i \cos\theta_j - \delta_{ij}\rangle \qquad (10)$$

where θ_i, $i \in \{x,y,z\}$, is the angle between the ith molecular axis and the bilayer normal, and the averaging is done over all lipids in the sample and over the sampling time. In our simulations, only completely unrestrained lipids were considered for averaging. The molecular axes are defined for each saturated carbon atom as follows: x is along the H–H vector, y is the bisectrix of the H–C–H angle, and z is defined as the vector perpendicular to the H–C–H plane.[21] For the unsaturated carbons the definition is slightly different, namely, z_k is along the vector from C_{k+1} to C_k (where k is the carbon index), x is perpendicular on the plane defined by the H–C vector and the z_k-axis, and y is perpendicular to the plane defined by x and z_k.[60] The experimentally observed deuterium order parameter S_{CD} can be computed using the relation[23]

$$S_{CD} = {}^2/_3 S_{xx} + {}^1/_3 S_{yy} \qquad (11)$$

If the molecular motion is such that isotropic rotation around the molecular z-axis occurs, then $S_{zz} = -2S_{xx} = -2S_{yy}$ and $S_{CD} = -{}^1/_2 S_{zz}$.[20] S_{zz} is also sometimes referred to as local S_{chain} or S_{mol}. The coordinates for the hydrogen atoms, which are not directly available as we employ the united atom model for all hydrocarbon atoms, have to be generated for this computation in the usual way (e.g., by using X-PLOR). For computation of the time averages, configurations were sampled every 128 fs. Extreme cases of the order parameter are $-S_{CD} = 0.5$ for the extended all-*trans* configuration (completely ordered state) where the chain is aligned along the bilayer normal ($\theta_i = 90°$, $i \in \{x,y\}$) and $-S_{CD} = 0$ if the hydrocarbon groups do not show any preferred orientation (complete disorder).

Diffusion Constant. The self-diffusion constant D is determined by the long time behavior of the mean square displacement ξ of a molecule. According to continuum diffusion theory, the diffusion constant in d dimensions is defined as[61]

$$D = \frac{1}{2d}\lim_{t\to\infty}\frac{\mathrm{d}}{\mathrm{d}t}\langle\xi^2(t)\rangle \qquad (12)$$

In our case, the two dimensional lateral square displacement $\xi^2_{lat}(t)$ and the one dimensional transversal square displacement $\xi^2_{tra}(t)$ are

$$\xi^2_{lat}(t) = (X^{CM}(t+t_0) - X^{CM}(t_0))^2 + (Z^{CM}(t+t_0) - Z^{CM}(t_0))^2$$

$$\xi^2_{tra}(t) = (Y^{CM}(t+t_0) - Y^{CM}(t_0))^2 \qquad (13)$$

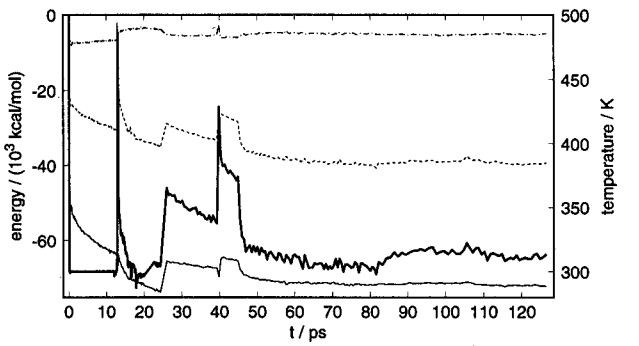

Figure 4. Energies and temperature during the equilibration simulation: (- -) total energy, (—) Coulomb energy, (– · –) van der Waals energy, and temperature (▬). During the initial 0.01 ps, the energies and temperature reached maximum values of $E_{tot.} = 8.0 \times 10^3$ kcal/mol, $E_{vdW} = 3.1 \times 10^3$ kcal/mol, $E_{Coul} = -45.4 \times 10^3$ kcal/mol, and $T = 559$ K (some peaks outside plot range), as a result of the high potential energy of the original setup. The other peaks in the energy and temperature curves resulted from rescaling of the reference positions, i.e., from the corresponding addition and subsequent dissipation of mechanical energy.

Here, X^{CM}, Y^{CM}, and Z^{CM} are the Cartesian coordinates of the center of mass of the lipid, and t_0 is a point of reference along the simulated trajectory.

We determined the curves of square lateral and transversal displacements by averaging eqs 13 over all completely unrestrained lipid molecules. Let $\mathcal{L}_0$ be the set of the latter molecules. To reduce the statistical error, we introduced a further averaging procedure over the set $\{t_0\}$ of all possible reference times. The curve of the mean squared transversal displacement was then calculated according to

$$\langle\xi^2_{tra}(t)\rangle = \frac{1}{N_0}\sum_{i\in\mathcal{L}_0}\frac{1}{M_0}\sum_{t_j\in\{t_0\}}(Y_i^{CM}(t+t_j) - Y_i^{CM}(t_j))^2 \qquad (14)$$

Here, N_0 and M_0 are the number of unrestrained lipids and the number of reference times, respectively. The same averaging was applied to the lateral displacement. The lateral and transversal diffusion constants were then determined from the asymptotic slopes of the corresponding $\xi^2(t)$ curves for "longer" times, formally for $t \to \infty$, in accordance with eq 12.

Obviously, the average transversal displacement $\langle\xi^2_{tra}(t)\rangle$ must approach a constant value in the limit $t \to \infty$ if the bilayer is not to disintegrate, which means that the long time transversal diffusion constant must vanish in the present case. However, for a time domain in the range of a few picoseconds, the average transversal displacement curve can be expected to have a nonvanishing slope resulting from diffusion within a potential well that is preventing the lipids from leaving a monolayer. With a system of limited size, similar considerations hold true for the lateral diffusion and displacement. In the present study, however, the considerable lateral dimension of the bilayer of 85 × 100 Å^2 justifies the assumption that finite size effects on the lateral displacement can be neglected within a 100-ps time frame.

Results

Equilibration and Volume Adjustment. After the construction, we performed a 120-ps simulation of the membrane–water system in order to equilibrate the assembly and to achieve a low internal pressure that was in agreement with the estimates made for pressure due to surface tension (see Methods). The nonbonded energies, total energy, and temperature of the bilayer during the equilibration are shown in Figure 4. The pressure on the two water caps as determined by the boundary method is given in Figure 5.

Energies. We started the equilibration with all atom velocities equal to zero. During the first 12.9 ps, all atoms were coupled to a heat bath[62] in order to instantly remove excess heat from the

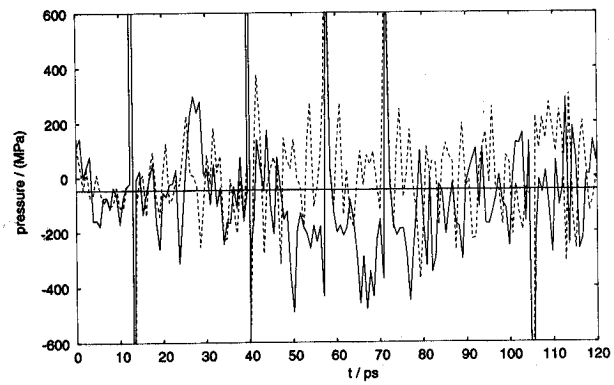

Figure 5. Pressure on the two water cap boundaries during the equilibration simulation: (—) pressure on the upper ($y > 0$) and (- -) pressure on the lower ($y < 0$) boundary. The pressure was determined using the boundary method, eq 3. The horizontal line marks the mean value of –46.7 ± 12.8 MPa. As with the energies, peaks in the pressure curve beyond the fluctuation level resulted from rescaling of the reference positions of boundary atoms.

system. During all other times, heat was only exchanged through the stochastic boundary. The global coupling to a heat bath successfully reduced the temperature to 300 K within 0.2 ps and led to a very small fluctuation level of the temperature during the first 12.9 ps. The effect of the coupling to a heat bath through the stochastic boundary at times $t > 12.9$ ps can be seen as the temperature repeatedly decreases from high values caused by rescaling of the atom reference positions (see below). The coupling time of this heat exchange through the boundary can be estimated from Figure 4 to be of the order of 20 ps and reflects the time required for conducting heat from the inside of the system to the surface.

Similar to the temperature, the energies show sharp peaks caused by the repeated rescaling of the reference positions of boundary atoms. The very fast relaxation of these energy peaks, within about 1 ps, results from the identity of the location where mechanical energy is added to the system and where heat is extracted from it, namely, the boundary. Superimposed on the discontinuities and fast relaxations related with the rescaling events, the Coulomb energy and consequently the total energy undergo a slow relaxation with a characteristic relaxation time of about 50 ps. In contrast, the van der Waals energy does not show a similar slow relaxation. The relaxation of Coulombic and total energy reflects a structural change of the lipids, especially the lipid head groups, and the adjustment of the water caps. Figure 4 shows that the bilayer–water system has reached equilibrium at the end of the simulation.

Pressure. While running the simulation, we found that the pressure on the boundary surfaces (see Methods) was predominantly negative, i.e., the average positions of boundary atoms were shifted toward the inside of the system when compared to the reference positions. Because the pressure, especially on the two water caps, averaged over a time interval of 20 ps was at times deviating from –39 MPa, the estimate made for the pressure due to surface tension (see Methods), we changed the volume of the system several times by rescaling of the reference positions of boundary atoms. The rescaling factors, rescaling axes, and rescaling times were as follows: (0.98, *xyz*, 12.9 ps); (0.98, *y*, 24.6 ps); (0.98, *y*, 39.8 ps); (0.99, *y*, 57.7 ps); (0.99, *y*, 71.6 ps); (1.02, *y*, 105.1 ps). Except for the first rescaling event, where all three coordinates were rescaled, only the *y*-coordinates of the reference atoms and, therefore, only the thickness of the bilayer were affected. Each rescaling step led to a sharp increase or decrease of the boundary pressure which was very short lived, with the pressure returning to the normal fluctuation level within less than 1 ps (see Figure 5). After some of the rescaling events, e.g., the rescaling at $t = 12.9$ ps, we observed an overshooting of the boundary pressure value in a direction opposite to the direction of the initial peak. Rescaling of the reference positions, therefore, induces a damped oscillation in the boundary.

Despite the repeated changes of the atom reference positions and the structural changes of the lipids accompanying equilibration, the pressure averaged over a 20-ps interval showed very little change when compared to the fluctuation level of the boundary pressure values. We also calculated the average of the water cap boundary pressure over the whole equilibration and found that its value, –47 MPa, is in good agreement with the value estimated to result from surface tension alone, –39 MPa. Note that the large negative pressure on the two water caps is present mainly because of the curvature of their vacuum boundary in the equilibration setup (see Figure 3). Other MD simulations of membrane systems report pressures of the order of –1 MPa[16] and +25 MPa,[21] i.e., values that are also in the megapascal range. We conclude that the pressure in the bilayer–water system, within a margin of about 10% of the volume enclosed by the stochastic boundary, is essentially constant and that the packing of the system during equilibration corresponds to a low internal pressure. One reason for this may be the relatively "soft" nature of the harmonic restraining potential which allows the boundary atoms to adjust their positions depending on the pressure, as opposed to the situation of a periodic boundary simulation where the periodic cell dimensions have a more dramatic effect on the pressure in the system.

Simulation I. After the equilibration, we switched to a new set of partial charges which we took from the parameter and topology file CHARMM22 of CHARMm provided to us by A. MacKerell of the Department of Chemistry at Harvard.[53] We started the simulation with the structure, atom velocities, and atom reference coordinates of the end of the equilibration. The reference coordinates were left unchanged during simulation I.

Energies. The change of the charge parameter set caused the system to be off equilibrium at the beginning of the simulation, with especially the temperature reaching a maximum of 388 K within the first picosecond. As can be seen from Figure 6, return to equilibrium required about 30 ps. During the final 25 ps of simulation I, which were used for analysis, the nonbonded energies as well as the temperature exhibit only minor fluctuations around their mean values, indicating that equilibrium has been reached.

Pressure. The pressure on the two water caps (see Figure 7) was evaluated according to the boundary method, eq 3. The pressure shows strong fluctuations around a mean value of –55.7 ± 3 MPa. This value is slightly lower than the pressure during the equilibration, which was –46.7 MPa. One reason for the decrease of the pressure may have been an improved interaction between lipid head groups and water due to the change of the lipid partial charge set at the beginning of simulation I. An inspection of the pressure curves in Figure 7 suggests that the two water cap pressures are anticorrelated, even though the correlation coefficient of the two pressures is only –0.3. The anticorrelation implies that the whole assembly performs an oscillation within the potential of the harmonic restraints on the boundary.

Diffusion. In order to calculate the diffusion coefficients of POPC, we determined the average displacement of the center of mass of the lipids. The average displacement curves in Figure 8 exhibit two different time domains: a short-time domain from 0 to 2 ps and a long-time domain from 4 to 25 ps with different diffusion behavior. From a linear regression fit to the $\langle \xi^2 \rangle$ curves in Figure 8, we determined according to eq 12 $D^l_{lat} = 0.023 \times 10^{-5}$ cm^2/s as the lateral and $D^l_{tra} = 0.115 \times 10^{-5}$ cm^2/s as the transversal long-time diffusion constants. In a similar way, we determined the short-time diffusion constants for the time range up to 2 ps as $D^s_{lat} = 0.296 \times 10^{-5}$ cm^2/s and $D^s_{tra} = 0.499 \times 10^{-5}$ cm^2/s. These values of the diffusion constants are of the same order of magnitude as experimental findings for a 1,2-dipalmitoyl-*sn*-glycero-3-phosphatidylcholine (DPPC) membrane containing 12 wt % water (the back-scattering spectroscopy used in the

TABLE I: Simulation Parameters Used for Simulation II[a]

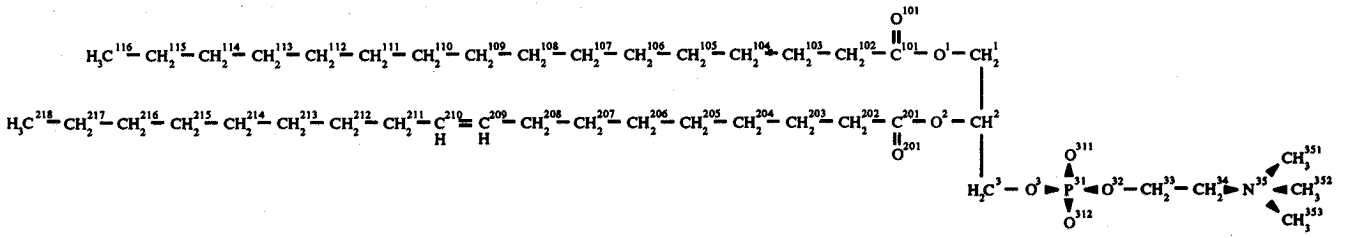

atom	q/e	ϵ/(kcal/mol)	σ/Å	$\epsilon_{1:4}$/(kcal/mol)	$\sigma_{1:4}$/Å	atom	q/e	ϵ/(kcal/mol)	σ/Å	$\epsilon_{1:4}$/(kcal/mol)	$\sigma_{1:4}$/Å
C351	0.40	0.1811	3.8576	0.1000	3.3854	C110	0.00	0.1142	3.9823	0.1000	3.3854
C352	0.40	0.1811	3.8576	0.1000	3.3854	C111	0.00	0.1142	3.9823	0.1000	3.3854
C353	0.40	0.1811	3.8576	0.1000	3.3854	C112	0.00	0.1142	3.9823	0.1000	3.3854
N35	–0.60	0.2384	2.8510	0.2384	2.8510	C113	0.00	0.1142	3.9823	0.1000	3.3854
C34	0.40	0.1142	3.9823	0.1000	3.3854	C114	0.00	0.1142	3.9823	0.1000	3.3854
C33	0.10	0.1142	3.9823	0.1000	3.3854	C115	0.00	0.1142	3.9823	0.1000	3.3854
O32	–0.55	0.1591	2.8509	0.1591	2.8509	C116	0.00	0.1811	3.8576	0.1000	3.3854
P31	1.50	0.0903	3.2070	0.0903	3.2070	O201	–0.52	0.1591	2.8509	0.1591	2.8509
O311	–0.80	0.6469	2.8509	0.6469	2.8509						
O312	–0.80	0.6469	2.8509	0.6469	2.8509	C201	0.63	0.1200	3.7418	0.1000	3.3854
						C202	0.10	0.1142	3.9823	0.1000	3.3854
O3	–0.55	0.1591	2.8509	0.1591	2.8509	C203	0.00	0.1142	3.9823	0.1000	3.3854
C3	0.10	0.1142	3.9823	0.1000	3.3854	C204	0.00	0.1142	3.9823	0.1000	3.3854
C2	0.13	0.0486	4.2140	0.1000	3.3854	C205	0.00	0.1142	3.9823	0.1000	3.3854
O2	–0.34	0.1591	2.8509	0.1591	2.8509	C206	0.00	0.1142	3.9823	0.1000	3.3854
C1	0.13	0.1142	3.9823	0.1000	3.3854	C207	0.00	0.1142	3.9823	0.1000	3.3854
O1	–0.34	0.1591	2.8509	0.1591	2.8509	C208	0.00	0.1142	3.9823	0.1000	3.3854
						C209	0.00	0.0903	3.2070	0.0903	3.2070
O101	–0.52	0.1591	2.8509	0.1591	2.8509	C210	0.00	0.0903	3.2070	0.0903	3.2070
C101	0.63	0.1200	3.7418	0.1000	3.3854	C211	0.00	0.1142	3.9823	0.1000	3.3854
C102	0.10	0.1142	3.9823	0.1000	3.3854	C212	0.00	0.1142	3.9823	0.1000	3.3854
C103	0.00	0.1142	3.9823	0.1000	3.3854	C213	0.00	0.1142	3.9823	0.1000	3.3854
C104	0.00	0.1142	3.9823	0.1000	3.3854	C214	0.00	0.1142	3.9823	0.1000	3.3854
C105	0.00	0.1142	3.9823	0.1000	3.3854	C215	0.00	0.1142	3.9823	0.1000	3.3854
C106	0.00	0.1142	3.9823	0.1000	3.3854	C216	0.00	0.1142	3.9823	0.1000	3.3854
C107	0.00	0.1142	3.9823	0.1000	3.3854	C217	0.00	0.1142	3.9823	0.1000	3.3854
C108	0.00	0.1142	3.9823	0.1000	3.3854	C218	0.00	0.1811	3.8576	0.1000	3.3854
C109	0.00	0.1142	3.9823	0.1000	3.3854						

[a] The charges have been taken from the parameter file of Charmm22,[53] while the van der Waals parameters have been taken from the X-PLOR file param19.pro[46] and from *ChemNote* (within *Quanta*[50]).

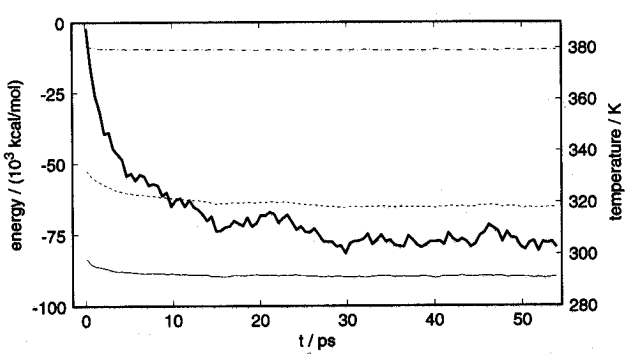

Figure 6. Energies and temperature during simulation I: (- -) total energy, (—) Coulomb energy, (– · –) van der Waals energy, and (—) temperature. The final 25 ps of the simulation were used for analysis.

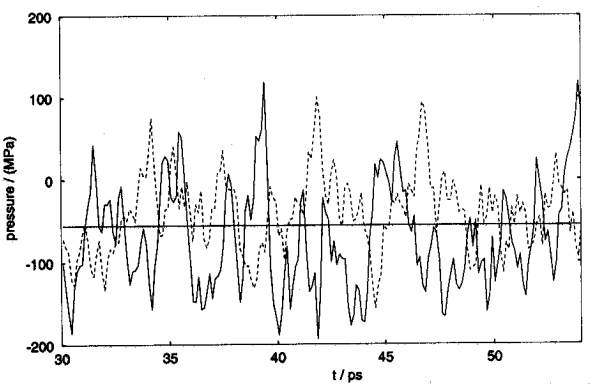

Figure 7. Pressure on the two water cap boundaries during simulation I: (—) pressure on the upper ($y > 0$) and (- -) pressure on the lower ($y < 0$) boundary. The pressure was determined using the boundary method, eq 3. The horizontal line marks the mean value of –55.7 ± 3 MPa.

experiment covers motions with relaxation times of 10^{-10}–10^{-8} s, which is barely in the range of our simulations) reported in ref 5: $D^{l}_{lat} = 0.0097 \times 10^{-5}$ cm^2/s, $D^{s}_{lat} = (0.015\text{–}0.6) \times 10^{-5}$ cm^2/s, and $D^{s}_{tra} = 0.21 \times 10^{-5}$ cm^2/s. However, König et al. note that these diffusion coefficients "should be handled with care" as the underlying model assumptions are an oversimplification (König et al. assume in their model that the proton motions in the fatty acid tail of a lipid are completely independent of each other, which is of course not valid for protons within one molecule), and furthermore their measurements were done on a DPPC sample in the liquid-crystalline phase.[63]

Area per Head Group. Using the procedure described in Methods, we determined the average area per POPC head group at the end of simulation I as $A = 46.3 \pm 0.01$ Å^2. Nagle and Wiener[38] determined experimental values of the average area per DPPC head group in three different membrane phases: for the crystal phase (L_c) at 0 °C $A = 45.8$ Å^2, for the gel phase ($L_{\beta'}$) at 20 °C $A = 48.5$ Å^2, and for the fluid phase (L_α) at 50 °C $A = 57.6$–70.9 Å^2. Wiener and White[51] give experimental values for DOPC of $A = 40$ Å^2 in the crystalline all-*trans* phase and $A = 60$ Å^2 in the liquid-crystal phase (L_α). Since POPC differs from DPPC through the addition and from 1,2-dioleoyl-*sn*-glycero-3-phosphatidylcholine (DOPC) through the deletion of one double bond segment (–CH=CH–), one can expect that the average area per head group of POPC is between those for DPPC and DOPC. A comparison, therefore, suggests that the bilayer during simulation I which was done at $T = 27$ °C is in the crystal or gel phase.

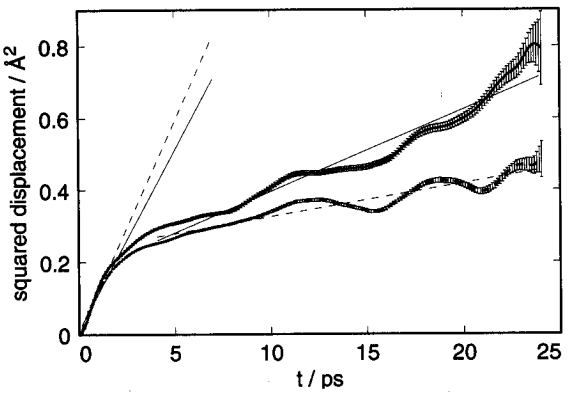

Figure 8. Transversal (—, upper curve) and lateral (- -, lower curve) average square displacement $\langle \xi^2 \rangle$ of the center of mass of a lipid molecule in the bilayer water system during simulation I. The error bars show the standard deviation of the displacement values (see eq 14). The straight lines result from a linear regression fit to the $\langle \xi^2 \rangle$-curves in two different time domains (see text).

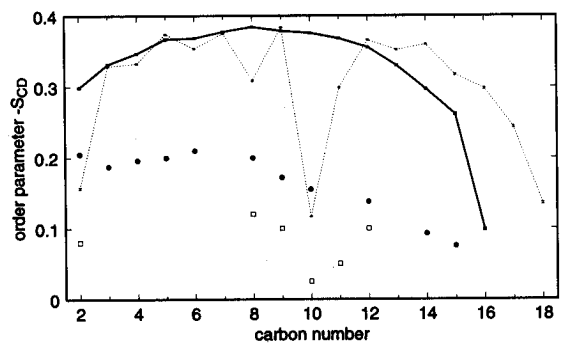

Figure 9. Deuterium order parameter profile of the sn-1 (—) and sn-2 chain (- -) of POPC as determined from simulation I. For comparison, the experimental results of ref 64 for the palmitoyl chain (●) and for the oleic chain (□)[65] of POPC in the fluid phase at 27 °C are also given. The abscissa refers to a numbering scheme where the fatty acid carbons are numbered consecutively, starting with 1 at the ester carbon. Error bars indicating the standard deviation of the simulation values are too small to be represented.

Order Parameters. We determined the order parameter profile of both fatty acid tails of POPC (see Figure 9). For the unsaturated oleoyl tail, we found a pronounced odd–even alteration of the order parameter as a function of carbon number which is not present in the profile of the saturated palmitoyl chain. Both profiles show a plateau which is also observed in experiments,[37,64,66] even though the decrease of the experimental order parameter $-S_{CD}$ toward the end of the palmitoyl chain begins at a lower carbon number than in the calculated profile. The absolute value of the calculated order parameters in Figure 9 is about two times larger than the absolute value of the experimental order parameters which were determined from POPC in the fluid phase. For carbon number 2 the absolute value of the simulated order parameters are lower than those for carbon number 3, while the opposite is true for the experimental values. The comparison of the calculated with experimental order parameter profiles indicates that during simulation I, the simulated bilayer was not in the liquid crystal phase but rather in the gel phase, where the molecular order is higher. Unfortunately, no experimental data on the gel phase are available for comparison.

Both the experimental data and our simulation data show a characteristic dip in the order parameter profile for the second double bonded carbon atom (C9). As pointed out in ref 60, two factors contribute to the order parameter (see eq 10): (i) the orientation of the C–H bond vector, expressed through the angle θ with the bilayer normal (see Figure 10) and (ii) the orientational fluctuations of the C–H bond vector. The method of MD simulations allows measurement of each factor independently and, therefore, establishes which contribution dominates.

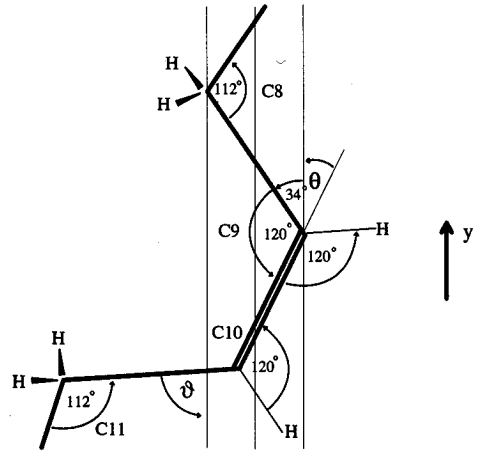

Figure 10. Sketch of the idealized geometry of the vicinity of the *cis*-double bond. It is assumed that the segments from C2 to C8 are prefectly aligned with the bilayer normal (vertical lines). Angles of 112° and 120° have been assumed for sp^3 and sp^2 hybridization of carbon atoms, respectively.[60]

The average angle of the double bond with the bilayer normal was determined for the upper layer at $\theta_u = 23.22 \pm 0.14°$ and for the lower layer at $\theta_l = 22.17 \pm 0.13°$. These values are less than what one would expect ($\theta = 26°$) for a perfect (except for the *cis*-double bond) all-*trans* chain with the segment from C2 to C8 perfectly aligned with the bilayer normal (see Figure 10). The high values of the order parameter $-S_{CD} \approx 0.4$, close to the highest value of $-S_{CD} = 0.5$, indicate that these segments are indeed highly ordered and well aligned with the bilayer normal. The average angle of the bond segment C10–C11 was determined for the upper layer at $\vartheta_u = 57.05 \pm 0.20°$ and for the lower layer at $\vartheta_l = 62.41 \pm 0.19°$. Again these values are lower than what one would expect for a perfect geometry ($\vartheta = 86°$). This deviation is a result of the tight packing in the gel phase which tends to realign the hydrocarbon segments C11 to C18 with the bilayer normal and hence changes the angles in the observed fashion.

The local chain order parameter is $S_{zz} = 0.7541 \pm 0.0013$ for the C=C bond and $S_{zz} = -0.0478 \pm 0.0018$ for the following C10–C11 segment. This is in good agreement with values computed only from the average angles θ and ϑ given above, namely, for the C=C bond $S_{zz}(\theta) = 0.76$ to 0.79 and for the following C10–C11 segment $S_{zz}(\vartheta) = -0.05$ to -0.18. This confirms the conclusion of ref 60 that the dip in the order parameter profile is not due to increased fluctuations but that it is rather a pure geometric effect.

Distribution of Molecular Groups. A recent publication of Wiener and White[51] provides detailed structural information about fluid DOPC bilayers that can readily be used for comparison with our simulation. We use a similar parsing scheme as described by Wiener and White (see Figure 1). One obvious difference is that we have a palmitoyl chain instead of an oleoyl chain at the sn-1 position. When comparing the calculated density profiles of lipid segments (see Figure 11) with the experimental profiles shown in Figures 18b and 19b, it becomes evident that the bilayer is much thicker in simulation I than in the liquid-crystal phase that was measured in the experiment. The pronounced dip in the CH_2 distribution at the center of the bilayer in Figure 11a shows that there is little overlap of the tails of the two monolayers. The two dips in the CH_2 distribution of the sn-2 chain at ±12 Å coincide with the peaks of the double bond distributions as both have the same origin, namely, the substitution of a $-CH_2CH_2-$ segment by a $-CH{=}CH-$ segment. The sn-2 oleoyl chain, which is two carbon segments longer than the sn-1 palmitoyl chain, has not only a higher density of CH_2 groups than the palmitoyl chain at the center of the bilayer (7.7×10^{-3} Å^3 compared to 6.4×10^{-3} Å^3), but it also extends about 1.76 Å further toward the head group region.

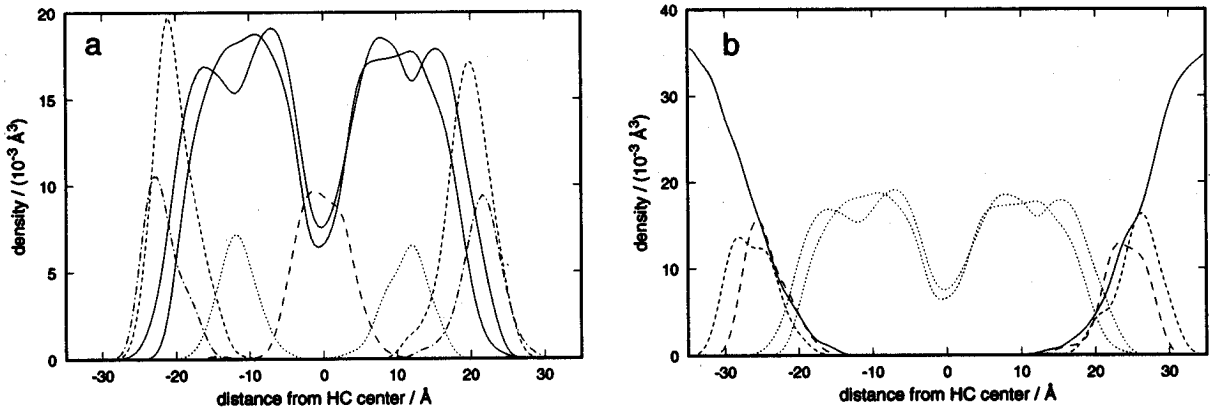

Figure 11. Cross-membrane density profiles of atom groups of the bilayer–water system as specified in Figure 1: (a) (lipid tail region) methylene groups (CH_2, —) of the sn-1 and sn-2 chain, methyl groups (CH_3, – –), ester groups (- -), double bonded carbons (···), and glycerol backbone (– · –); (b) (head group and water region) water (—), choline (- -), and phosphate (– –). The methylene groups (···) are shown as a reference. The profiles were calculated by averaging static profiles (see Methods) over the last 25 ps of simulation I.

Two Disasters. The analysis of simulation I led to the conclusion that the simulated bilayer is in the gel phase rather than the liquid-crystal phase, which is the biologically most relevant phase.[36] Perhaps the most important difference between the bilayer of simulation I and experimental data on liquid-crystal phase bilayers is the area per lipid molecule, which is too small by a factor of 1.5. We, therefore, decided to increase the area per lipid molecule from 46.3 Å², the value during simulation I, to the experimental value known for the liquid-crystal phase, namely 70 Å² [10,51] and eventually induce a phase change in the system as an effect of the surface area increase. In the following, we report on two attempts at inducing this change which we deemed unsuccessful.

"Disaster I": Separation of the Monolayers. In our first attempt to increase the area per lipid molecule by a factor of 1.5, we rescaled the x- and z-coordinates of the reference positions that were used during simulation I by a factor of 1.23 while leaving the y-coordinates unchanged. We, thereby, increased both the lateral area and the volume of the system by a factor of 1.5, intending to readjust the bilayer thickness and internal pressure at a later time.

We started the simulation using the final structure and atom velocities of simulation I and using the rescaled reference positions to calculate the restraining forces on atoms. During the simulation, we monitored energies and boundary pressure in the system. Initially, the restraining energy was increased by 11 300 kcal/mol when compared to the energy at the end of simulation I. As a consequence of this relatively small perturbation (compare "Disaster II") the temperature raised to a moderate maximum value of 340 K after 0.1 ps of simulation time. The two nonbonded energies showed qualitatively different behavior: While the Coulomb energy decreased throughout the simulation, the van der Waals energy increased during the first 3 ps by 3000 kcal/mol and then decreased by 600 kcal/mol until the end of the simulation. During disaster I, therefore, the system never regained the van der Waals energy lost during the initial phase of structural reorganization which indicates a disruption of good contacts in the lipid tail region.

After the system had reached equilibrium, we displayed the structure on a graphics terminal and found that, except for the lipids in the boundary which were restrained, the two monolayers had separated (see Figure 12). From this, it became clear that a volume increase by 50% was, even for a short time interval of the order of 10 ps, beyond the limit of what the system could adjust to while preserving the integrity of the bilayer. Despite the ability of the stochastic boundary to compensate volume changes in a 10% range (see Equilibration), the low internal pressure in the system led to the creation of a hole at the location of weakest interaction between molecules, namely, the area of van der Waals contact between the monolayers. We concluded that all further changes in the setup of the system should meet the requirement of volume conservation.

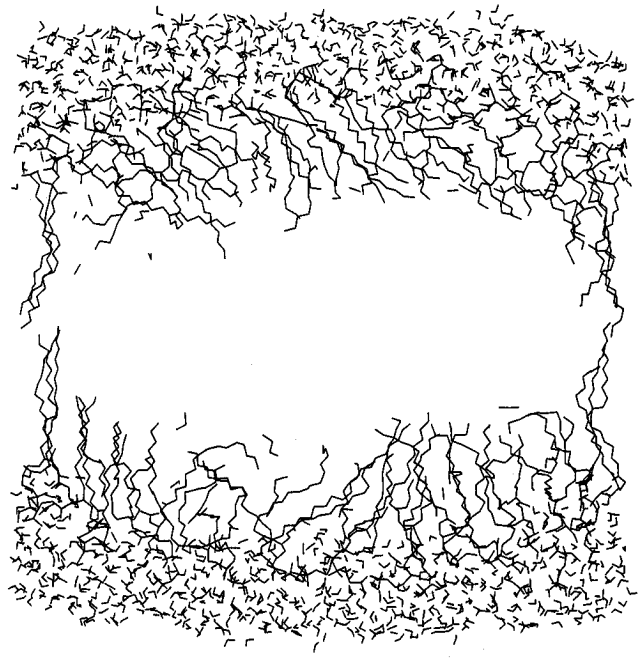

Figure 12. Line drawing of molecules within a 20-Å slice through the membrane–water system at the end of the disaster I simulation. The slice is parallel to the xy plane. Only atoms for which the z-coordinates satisfy $|z| < 10$ Å are shown, such that some of the molecules appear incomplete.

"Diaster II": Thermal Disintegration. In our second attempt to increase the average area per POPC head group, we rescaled the x- and z-coordinates of the atom reference positions by a factor 1.23 and the y-coordinates of the reference positions by 0.66 before starting the simulation, thus keeping the volume of the system constant. We also changed the restraining force constants on lipid atoms. Only the phosphorus atoms of the lipids were subject to a restraining potential, with the maximum force constant k_{max} reduced by a factor 5 (see Methods). We otherwise proceeded in exactly the same way as described in "Disaster I", above. Especially, the restraining potential with respect to the water caps was not changed.

After starting the simulation, we observed an initial 1-ps phase of interconversion of the restraint energy into other potential energies and heat, followed by a relaxation phase during which energies and temperature decreased rapidly. This time, the restraint energy at the beginning of the simulation was as much as 4×10^5 kcal/mol higher than the restraint energy at the end

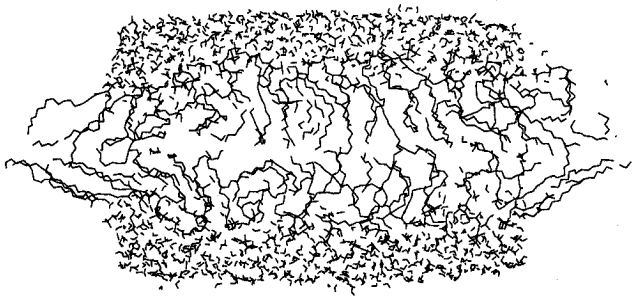

Figure 13. Line drawing of molecules within a 20-Å slice through the membrane–water system at the end of the disaster II simulation. The slice shown in parallel to the xy plane. Only atoms for which the z-coordinates satisfy $|z| < 10$ Å are shown, such that some of the molecules appear incomplete.

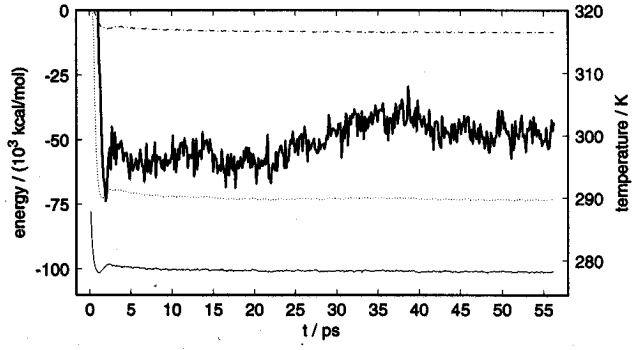

Figure 14. Energies and temperature during simulation II: (- -) total energy, (—) Coulomb energy (– · –) and (—) temperature. During the first picosecond, the energies and temperature reached maximum values of $E_{tot.} = 211.3 \times 10^3$ kcal/mol, $E_{vdW} = 0.53 \times 10^3$ kcal/mol, $E_{Coul} = -77.8 \times 10^3$ kcal/mol, and $T = 767.8$ K (some peaks outside plot range), as a result of the high potential energy of the setup after the induction of the phase transition. The final 46 ps of the simulation were used for analysis.

of simulation I, and the maximum temperature reached was 1020 K, compared to a maximum temperature of 340 K during diaster I.

When displaying the system after 3 ps of simulation time on a graphics screen, we observed two potentially pathological features of the structure: a large number of water molecules had escaped through the stochastic boundary, and, more importantly, the tails of lipid molecules in the lateral boundary region were pointing outward into the vacuum in a manner that looked very much like the result of an explosion (see Figure 13). Both the high temperature reached during the simulation and the distortion of the stochastic boundary after rescaling are possible reasons for the escape of unrestrained water molecules from the system. As a cause of the extreme distortion of lipid tails in the lateral boundary, we considered the change from restraining all lipid atoms in the boundary to restraining phosphorus atoms only. This idea, however, could be ruled out after analyzing simulation II (see below) in which the same restaining potential was used but no similar effect on the boundary lipids was observed. The extreme disorder of the boundary lipid tails was, therefore, also a consequence of the high temperature reached during the disaster II simulation, which in turn was caused by the high restraint energy at the beginning of the simulation. We did not continue the simulation beyond the 3 ps reported here even though the bilayer may have eventually reached a new equilibrium. Instead, we decided to proceed in a more cautious way when changing the system setup and to avoid restraint energy increases of the order of 15 kcal/mol per atom in the system which had proven to drive the system far from equilibrium.

Simulation II. To avoid high restraint energies in setting up simulation II, we performed a molecular rescaling (see Methods) of the x- and z-coordinates of both the reference positions and the actual atom positions as obtained at the end of simulation I. The scaling factor used for x and z was 1.23, leading to an expected increase of the lateral area by 50%. New water caps with a simple, rectangular geometry were added on both sides of the bilayer (see Construction of the Membrane Bilayer). We then rescaled the y-coordinates of all reference positions by a factor of 0.66 in order to guide the system to an equilibrium with volume and density equal to the values during simulation I. The main difference between the system setup of the disaster II simulation and of simulation II is the shifting in x- and z-direction of all atoms to locations near their respective reference positions, through molecular rescaling of the actual coordinates. After starting the simulation, this led to a total restraint energy in the system of 2×10^5 kcal/mol, which was only 50% of the restraint energy at the beginning of disaster II.

Energies. As had already been observed during the disaster simulations, the system needed time to adjust to the new setup. The nonbonded energies and the temperature decreased continuously during the first 10 ps of the simulation (see Figure 14), which is considered an equilibration phase. During the time from 10 to 56 ps of simulation II, which is used in the subsequent analysis, the energies and temperature show only typical equilibrium fluctuations.

Pressure. The values of the pressure on the top and bottom surface at the beginning of simulation II were very high (≈7500 MPa) because in this direction only the reference positions were rescaled. The pressures on the other surfaces deviate only slightly from their respective means, because in those directions the actual atom positions were also rescaled by molecular rescaling (see Methods). In the x- and z-directions, the average values of the pressure are –19.7 ± 0.54 MPa and –18.8 ± 0.42 MPa, respectively, which is approximately 16 MPa higher than the estimated contribution from the surface tension $p_{surf} \approx -36$ MPa. The average value of the pressure in the y-direction is –9.6 ± 0.53 MPa. This is about 46 MPa more than the average value in simulation I (–56 MPa), a difference that can be explained by the change from ellipsoidal to flat water caps with ideally no pressure contribution from surface tension. The fluctuations of the pressure on the six boundary surfaces, as depicted in Figure 15, are much smaller than those during the equilibration (see Figure 5) and simulation I (see Figure 7). We determined the correlation coefficients of the pressures on opposing surfaces and found a significant anticorrelation. For example, in the case of the two water cap boundaries the correlation coefficient was –0.72. The anticorrelation of pressures on opposing surfaces suggests that the whole system performs oscillations in the potential of the harmonic restraints.

Diffusion. The average displacement curves in Figure 16 exhibit two different time domains, similar to those observed in simulation I: a short-time domain from 0 to 2 ps and a long-time domain from 4 to 46 ps. From a linear regression fit to the $\langle \xi^2 \rangle$-curves in Figure 16, we calculated (eq 12) $D^l_{lat} = 0.073 \times 10^{-5}$ cm²/s as the lateral and $D^l_{tra} = 0.102 \times 10^{-5}$ cm²/s as the transversal long-time diffusion constants. Similarly, the short-time diffusion constants for the time range of up to 2 ps have been determined as $D^s_{lat} = 0.324 \times 10^{-5}$ cm²/s and $D^s_{tra} = 0.465 \times 10^{-5}$ cm²/s.

The long-time lateral diffusion constant D^l_{lat} has increased by a factor of 3 compared to its value in simulation I, while the other diffusion constants are of comparable size. Increasing the area per head group provided more room for the lipids to diffuse laterally, while it had only minor influence on the transversal diffusion. The short-time diffusion is also unaffected by the change from simulation I to simulation II.

It is not to be expected that lipids would exchange places ("hopping") on a time scale as short as the one covered by this simulation, as can be seen by estimating the time one lipid needs to explore the area per head group $A = 65.5$ Å² (see following section): $\tau = A/D^l_{lat} \approx 10$ ns. This estimate also agrees well with

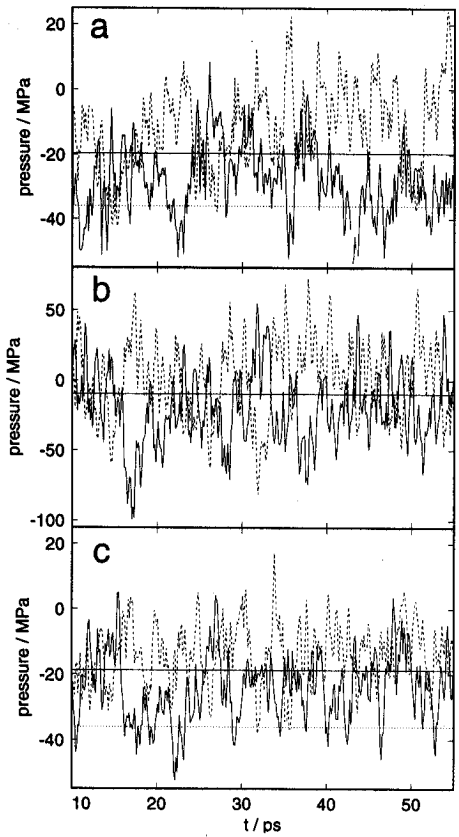

Figure 15. Pressure during simulation II on (a) the two lateral boundaries parallel to the *yz* plane, (b) the two water cap boundaries, and (c) the two lateral boundaries parallel to the *yx* plane: (—) pressure on the upper ($x, y, z > 0$) boundary and (- - -) pressure on the lower ($x, y, z < 0$) boundary, respectively. The pressure was determined using the boundary method, eq 3. The horizontal dotted line (···) in a and c marks the pressure due to surface tension in a bilayer with thickness R = 39 Å (peak to peak of choline distribution in Figure 19a, see Methods). The horizontal continuous lines (—) indicate the average values of the pressures.

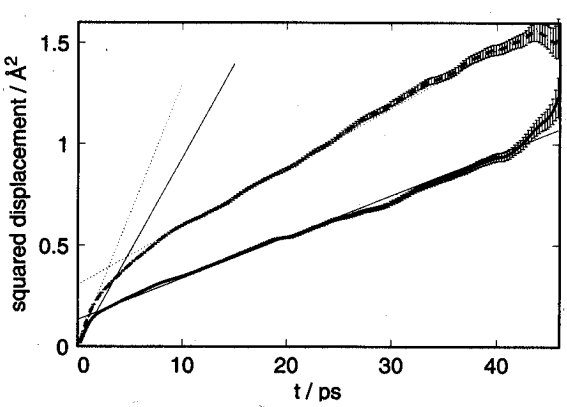

Figure 16. The transversal (—, lower curve) and lateral (- -, upper curve) average square displacement $\langle \xi^2 \rangle$ of the center of mass of a lipid molecule in the bilayer water system during simulation II. The error bars show the standard deviation of the displacement values (see eq 14). The straight lines result from a linear regression fit to the $\langle \xi^2 \rangle$-curves in two different time domains (see text).

the typical jump frequencies for lipids, which are in the order of $\nu \approx 10^7$–10^8/s.[67,68] If this time is divided by the number of simulated lipids N = 200, one obtains an estimate for the average time until one of the lipids in the patch will exchange its place with a neighbor $\tau/N \approx 45$ ps. Therefore one would expect to see only one event over the course of the simulation, which demonstrates that $D^{\perp}_{lat}$ does not describe the hopping of lipids.

Reference 67 reports a value of $D^{\perp}_{lat} = 0.07 \times 10^{-5}$ cm²/s for pyrene in DOPC at T = 30 °C in the liquid-crystalline phase,

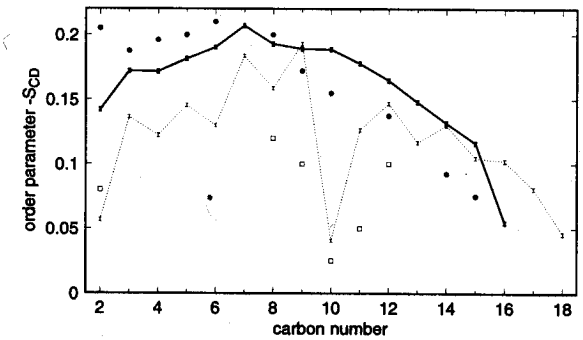

Figure 17. Deuterium order parameter profile of the sn-1 (—) and sn-2 chain (- -) of POPC as determined from simulation II. For comparison, the experimental results of ref 64 for the palmitoyl chain (●) and for the oleic chain (□)[65] of POPC in the fluid phase at 27 °C are also given. The abscissa refers to a numbering scheme where the fatty acid carbons are numbered consecutively, starting at the ester carbon with 1. Error bars indicate the standard deviation of the simulation values.

which translates through application of the free volume model of diffusion[69] to $D^{\perp}_{lat} = 0.036 \times 10^{-5}$ cm²/s as the self-diffusion coefficient for DOPC. Reference 68 reports $D^{\perp}_{lat} = 0.02 \times 10^{-5}$ cm²/s, $D^{\perp}_{tra} = 0.24 \times 10^{-5}$ cm²/s.

Area per Head Group. The lipid density is one of the adjustable parameters of the stochastic boundary simulation method. It can be predetermined by rescaling the reference positions. According to ref 70, the area per lipid for DPPC in excess water is A = 70 Å; the rescaling of the reference positions was done such as to achieve this value. However, in the course of the simulation, the area per head group stabilized at 65.5 ± 0.04 Å². This value is still in good agreement with the experimental values for the liquid-crystal phase of membranes. Nagle and Wiener[38] give experimental values for A for DPPC in the fluid phase (L_α) at 50 °C of A = 57.6–70.9 Å². Wiener and White[51,71] give experimental values for A for DOPC of A = 60 Å² in the liquid-crystal phase. Therefore, the density data given above support the conclusion that our sample (which is simulated at T = 27 °C) is in the liquid-crystal phase.

Order Parameters. There is good overall agreement between the order parameter profile calculated from simulation II (see eq 11) and the profile obtained in experiments.[64] However, the values for carbons close to the glycerol backbone are too low, while those toward the hydrocarbon end are too high (see Figure 17). This may be due to the short simulation time of only 56 ps, because profiles computed from shorter trajectories progressively approached the experimental values as the length of the trajectories increased. Compared to simulation I (cf. Figure 9), the values are now much closer to the experimental data for the liquid-crystal phase of POPC. As already observed in simulation I, the unsaturated oleoyl chain shows a strong odd–even alteration of the order parameter with carbon number, while the order parameters of the saturated palmitoyl chain do not exhibit this behavior. The increase in the order parameter for carbon atom number 2 which was observed in many experiments[64,72–74] is not reproduced by our simulation. However, order parameter profiles similar to the one reported here were previously obtained from other simulations.[22,23]

The average angle of the double bond with the bilayer normal was determined for the upper layer at θ_u = 37.96 ± 0.19° and for the lower layer at θ_l = 38.89 ± 0.20°. This value is larger than what would be expected (θ = 26°) for a perfect (except for the *cis*-double bond) all-*trans* chain with the segment from C2 to C8 perfectly aligned with the bilayer normal (see also Figure 10). However, the low values of the order parameter $-S_{CD} \approx 0.17$ indicate that the assumption of an alignment of tails and bilayer normal is not applicable to liquid-crystal bilayers. The increased area per head group, compared to simulation I, allows for more mobility of the hydrocarbon tails. This explains the

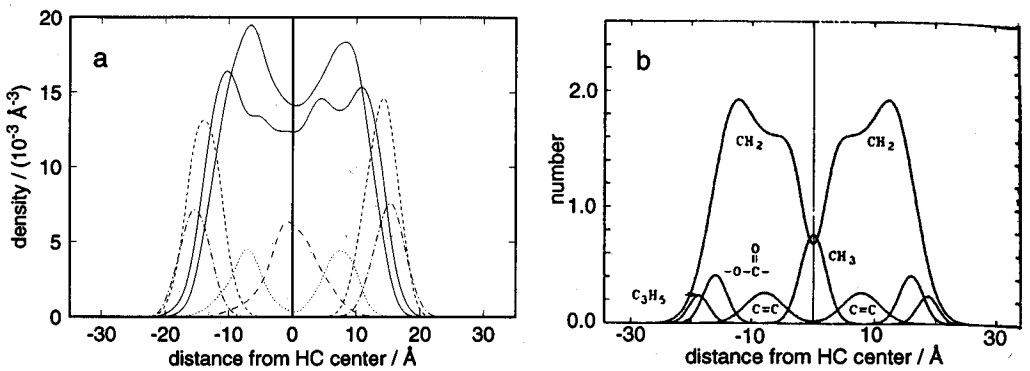

Figure 18. Cross-membrane density profiles of atom groups within the lipid tails as specified in Figure 1: methylene groups (CH_2, —) of the sn-1 and sn-2 chain, methyl groups (CH_3, – –), ester groups (- -), double bonded carbons (···), and glycerol backbone (– · –). The distance is measured relative to the center of the hydrocarbon (HC) area. (a) Profiles averaged over the last 46 ps of simulation II; (b) for comparison, experimental results for DOPC in number density units (figure adapted from ref 51).

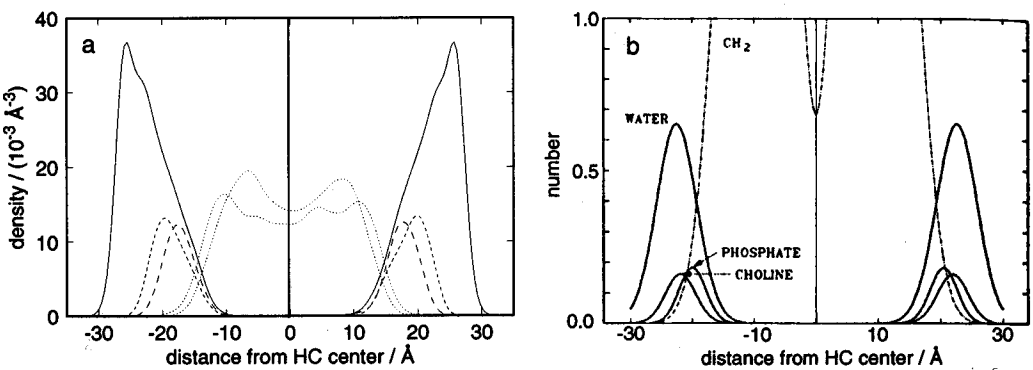

Figure 19. Cross-membrane density profiles of atom groups within the lipid head group region and of water as specified in Figure 1: (—) water, (- -) choline, and (– –) phosphate group. The methylene groups (···) are shown as a reference. The distance is measured relative to the center of the hydrocarbon (HC) area. (a) Profiles averaged over the last 46 ps of simulation II; (b) for comparison, experimental results for DOPC in number density units (figure adapted from ref 51).

larger value of $\theta \approx 38°$ compared to the value of 22.5° in simulation I. However, a value of $\theta \approx 38°$ does not agree with the value of $\theta = \pm 9°$ reported by ref 60 for liquid-crystal POPC bilayers at $T = 27$ °C.

The average angle of the bond segment C10–C11 with the bilayer normal was calculated for the upper layer at $\vartheta_u = 67.97 \pm 0.25°$ and for the lower layer at $\vartheta_l = 63.12 \pm 0.23°$. These values are lower than what would be expected for a perfect geometry ($\vartheta = 86°$); however, they are higher than the value obtained in simulation I ($\vartheta = 60°$). The deviation from the ideal-geometry value is due to the tight packing which tends to realign the hydrocarbon segments C11 to C18 with the bilayer normal, while the increase of θ and ϑ compared to simulation I is caused by the increase in lateral area per lipid, which reduces the tight packing found in the gel phase.

The local chain order parameter is $S_{zz} = +0.395 \pm 0.002$ for the C=C bond and $S_{zz} = -0.063 \pm 0.002$ for the following C10–C11 segment. This is in good agreement with values computed only from the average angles θ and ϑ given above, namely, for the C=C bond one finds $S_{zz}(\theta) = 0.41$ to 0.43 and for the following C10–C11 segment $S_{zz}(\vartheta) = -0.19$ to -0.29. Also, the result agrees well with the experimental value of $S_{zz} = 0.37 \pm 0.04$ reported by ref 60 for the C=C bond. Our simulation supports the conclusion of ref 60 that the dip in the order parameter profile is not due to increased fluctuations but that it is a geometric effect. However, the main conclusion of ref 60, namely, that the segmental fluctuations in POPC bilayers are not dependent on the segment geometry but are only determined by the distance of the segment from the lipid–water boundary, cannot be supported by our simulations (see below, section "Thermal Motion"). Instead, it can be stated that, with respect to the order parameter profile, the increased positional fluctuations of the double bonded carbons are overshadowed by an effect caused by the special geometry of the *cis*-double bond. Furthermore, only one double bonded carbon atom (C10) shows the strong dip in the order parameter profile, while both double bonded carbon atoms (C9, C10) have increased root mean square (RMS) values (see Figure 24). This also suggests that the dip in the order parameter profile for the double bonded carbon atom (C10) and the increased RMS values of both double bonded carbons are independent of each other.

Distribution of Molecular Groups. The distribution of molecular groups in our simulation (see Figures 18a and 19a) agrees well with the experimental results on DOPC of ref 51 (see Figures 18b and 19b). The maximum values, indicating the average positions of the quasimolecular fragments, are slightly closer to the center of the bilayer in our simulation than in the experiment. In our simulation the phosphate group on the average is located at +17.8 and –17.5 Å for the upper and lower layers, respectively, while ref 51 locates this group at 20.15 Å. The same applies to the choline group which can be found in our simulation at +19.3 and –19.1 Å for the upper and lower layers, respectively, while ref 51 finds a value of 21.86 Å. The pronounced dip in the CH_2 distribution at the center of the bilayer which was present in simulation I (see Figure 11a) has disappeared in simulation II, indicating a much stronger interdigitation of the two bilayers in the liquid-crystal phase compared to the gel phase. Compared to simulation I, the distribution of the double bonds has shifted toward the center of the bilayer. In agreement with the experimental data (see Figure 18b) there is a nonzero probability to find C=C segments at the bilayer center.

A major difference between parts a and b of Figure 18 is the distribution of the methylene groups relative to the head group. While Wiener and White see a substantial number of CH_2 groups extending beyond the glycerol backbone toward the solvent, in our simulation the CH_2 groups are not found beyond the backbone region.

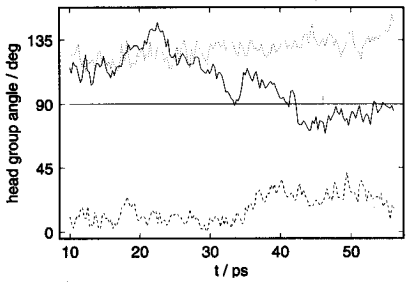

Figure 20. Fluctuations of head group orientation as given by the angle of the P–N vector with the bilayer normal. Shown are the trajectories of the head group angle for three extreme cases: (—) lipid 64 shows very strong fluctuation, (- -) lipid 116 has its head group almost upright most of the time, and (···) lipid 60 buries its head group in the hydrocarbon region. The horizontal line indicates an angle of 90° which corresponds to an orientation of the head group parallel to the membrane surface.

A comparison of Figure 19a,b shows that there is less water penetration into the head group region (choline and phosphate groups) in our simulation than suggested by the experimental data. This can be attributed to the short simulation time of 240 ps (this number includes the times of the equilibration, simulation I, and simulation II). The declining water density for distances of more than 32 Å from the center in Figure 19a marks the boarder of our simulation area, while the decrease in water density in Figure 19b marks the onset of the next membrane in a stack of multilamellar membranes.

Analysis of Head Group Region. We have determined the head group orientation as expressed by the average angle α between the P–N vector and the y-axis. For the upper layer we obtain $\alpha = 69.44 \pm 0.26°$ and for the lower layer $\alpha = 112.46 \pm 0.24°$. This translates into an azimuth of the head group above the bilayer plane of 20.56° and 22.46°, for the upper and lower layers, respectively, and is in excellent agreement with experimental data. Reference 75 reports that the head groups of POPC are found to be essentially parallel to the plane of the membrane, within 30°, while ref 76 reports that the P–N vectors of the two 1,2-dimyristoyl-*sn*-glycero-3-phosphatidylcholine (DMPC) molecules in the unit cell are inclined to the bilayer plane at angles of 17° and 27°. Reference 51 reports an angle of 22 ± 4° of the phosphocholine dipole with respect to the bilayer surface for DOPC in the liquid-crystal phase, and ref 77 find 18° for the liquid-crystal phase of DPPC. Our simulation shows that for POPC bilayers the head groups arrange in a similar fashion as previously found in experiments on DMPC and DOPC, namely, tilted toward the bilayer plane, pointing into the solvent with an inclination relative to the membrane plane of about 21°.

Two observations can be made from Figure 20, which shows the fluctuations of the head group angle of three different lipids over the course of the simulation: (i) the large magnitude of the fluctuations of the angle of up to 78° (lipid 64) on this short (ps) time scale and (ii) the great variation in head group orientations as illustrated by lipids 60 and 116. Lipid 116 has its head group almost vertical to the bilayer plane during the whole simulation, while the head group of lipid 60 points inward toward the hydrocarbon region of the membrane. These findings complement experimental results which have not been able to clearly identify the range of fluctuations in the head group orientation.[78]

The strong fluctuations and the wide range of possible head group angles are a major contribution to the surface roughness,[79,80] which can be observed, e.g., by atomic force microscopy.[81] The average y-position of the nitrogen atoms indicates the surface of the bilayer, and its RMS value is a measure of the surface roughness. From simulation II we obtained an average y-position of the N atom relative to the center of the bilayer of $Y_N = +19.08$ Å and $Y_N = -18.87$ Å with an RMS deviation of 2.39 and 2.33 Å for the upper and the lower monolayers, respectively. The average length of the P–N vector was determined at 4.11 ± 0.001 Å, which is shorter than the 4.3 and 4.5 Å reported by ref 76 for the two molecules in the unit cell of DMPC in the crystal phase.

Figure 21a shows that there is a very well defined surface of the lipid bilayer about 3.5 Å away from the average position of the nitrogen atom. Within 1 Å the count of head groups per box rises from 15 to over 200.

The source of the so-called "hydration force", a strong repulsive force felt at short distances of a few angstrom, between bilayers is not well understood. There is an ongoing discussion as to whether those forces are due to a structural rearrangement of water molecules close to the head groups (hydration forces)[82] or whether they are caused by steric interactions between the head groups of the two bilayers in contact (protrusion forces).[83] It is found experimentally that the repulsion decays exponentially with the distance ΔY between the two layers, according to

$$p = Ce^{-\Delta Y/\lambda} \tag{15}$$

where the decay length λ is close to 2 Å.

Reference 84 defines the protrusion or entropic contribution to the repulsive force per unit area between two bilayers as

$$p = T(\partial S/\partial \Delta Y)_T \tag{16}$$

The entropy S can be expressed by the configurational integral Z as $S = k_B \ln Z$, and Z factorizes into n identical "two-particle" configurational integrals z so that $Z = z^n$. n is the number of protrusion sites per unit area ($n \approx 1/A$ with $A = 65.5$ Å^2 the surface area per head group; see section "Area per Head Group") and

$$z = \int_0^{\Delta Y} dy_2 \int_{y_2}^{\Delta Y} dy_1 \, \rho(y_1) \tag{17}$$

where $\rho(y)$ is the density of independent protrusions extending to a height y above the membrane surface.

Reference 84 did not have available any data on ρ and therefore assumed an exponential dependency $\rho(y) = \rho(y_0)e^{-y/\lambda}$. However, $\rho(y)$ can be computed from our simulation and is plotted in Figure 21a. For simplicity we assume the same distribution of protrusions for both approaching surfaces and we also assume that this distribution is not changed as the two surfaces approach each other. The evaluation of the configurational integrals by numerical integration is then straightforward and the protrusion contribution to the repulsive force between two POPC bilayers can be computed by numerical differentiation according to eq 16. The resulting pressure is shown in Figure 21b for the simulation temperature $T = 300$ K.

The range of distances covered by our simulations (0–4 Å) has only a small overlap with the range (>3 Å) of observations in refs 84–86. The expected exponential dependency is present in the range $\Delta Y = 1$–3 Å, and a fit of eq 15 yields values of $\lambda = 2.0$ Å and $C = 179.9$ MPa, which are both in agreement with experimental data.[85,86] The more than exponential increase of the pressure for distances $\Delta Y = < 1$ Å is in agreement with the osmotic limit.[84] The pressure values for distances of more than $\Delta Y > 4$ Å are unreliable because the number of data points gathered from our simulation is too small for good statistics.

Figure 22, a ray-traced view of the top surface of the bilayer, can be compared to images obtained with an atomic force microscope, e.g., Figure 2 of ref 87. The head groups are clearly visible and show a fair amount of disorder. The disorder is also well illustrated by Figure 23, a side view of the upper monolayer. While most of the head groups are oriented parallel to the bilayer, some are in the upright conformation and others are buried in the hydrocarbon region.

Thermal Motion. Figure 24 shows the RMS value of the positional fluctuations of all lipid atoms in the three sections head group, backbone, and tails. First, the RMS values relative to the atomic coordinates of the average structure were computed from the last 46 ps of simulation II for every lipid independently.

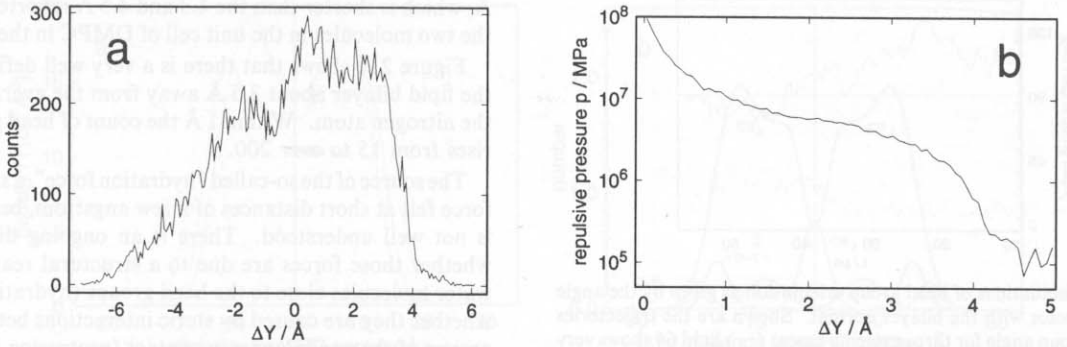

Figure 21. (a) Histogram of the distance ΔY at which the head group nitrogen is found relative to the average value. Data points were sampled every 128 fs over all unrestrained lipids. The average value was calculated at each time step to allow for a possible drift of the average. 200 boxes were used to cover the range of the abscissa. (b) Calculated repulsive steric protrusion pressure between two bilayers at separation ΔY if both bilayers have a distribution of protrusions as the one shown on the left side.

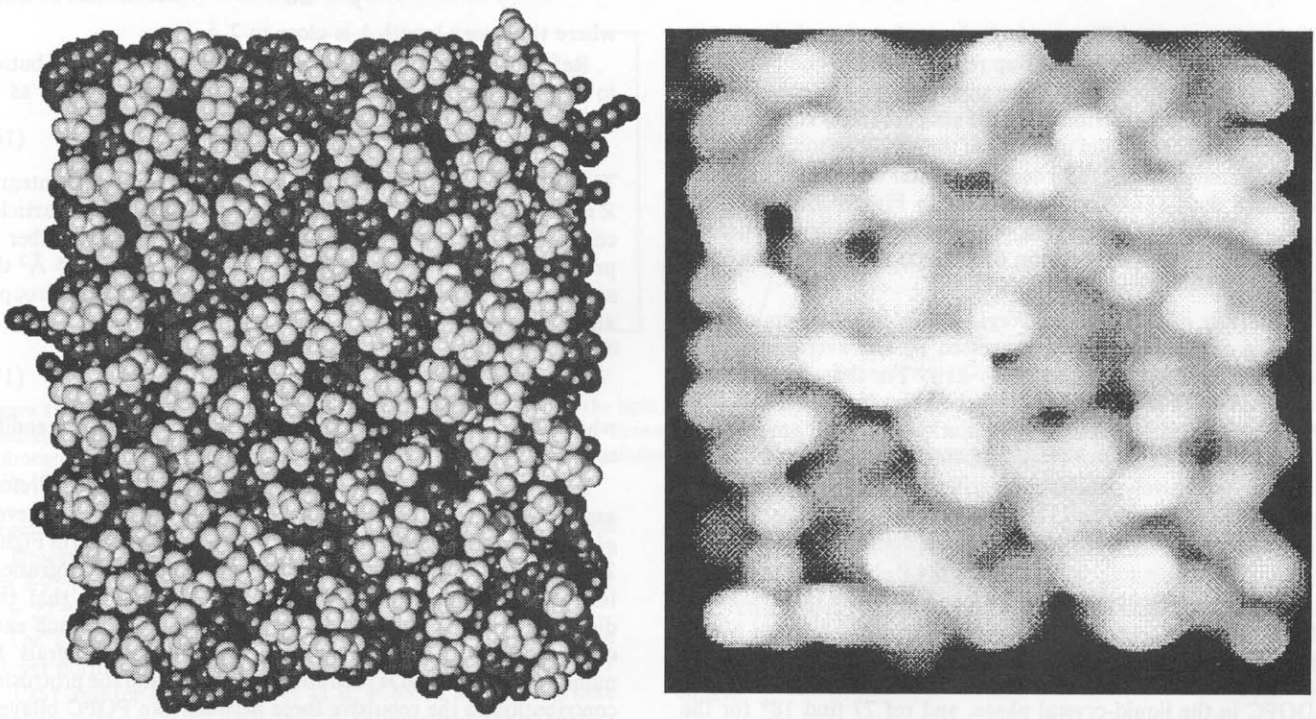

Figure 22. Surface of the upper half of the bilayer at the end of simulation II: (left) ray traced space filling model (the head groups are brighter colored than the backbone and the hydrocarbon part of the lipids; the water is omitted), (right) relief map (the height is grey-coded, lower points appearing darker).

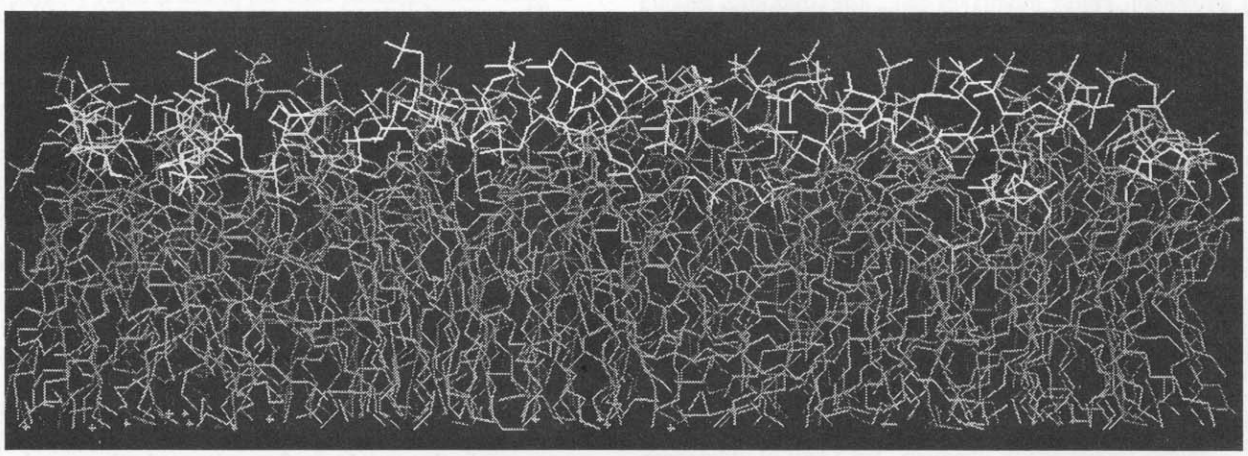

Figure 23. Side view of the upper half of the bilayer at the end of simulation II. The head groups are brighter colored than the backbone and the hydrocarbon part of the lipids; the water is omitted for clarity.

For each lipid atom, these RMS values were averaged over all unrestrained lipids and the standard deviations of the averages were determined.

The glycerol backbone is the most rigid part of the molecule; the flexibility increases toward both ends (head and tail), but the ends of the hydrocarbon tails are by far the most flexible part. This is consistent with crystallographic measurements,[88,89] NMR results,[90,91] incoherent quasi-elastic neutron scattering,[5] and joint

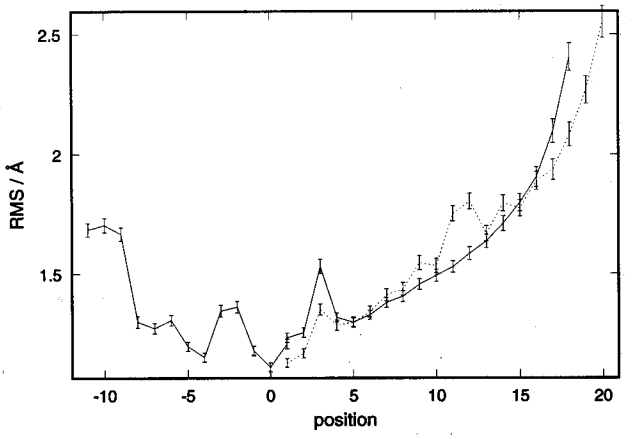

Figure 24. RMS deviation of lipid atoms from their average positions during simulation II. The RMS values were calculated using structures every 128 fs along the trajectory and then averaged over all unrestrained lipids. The error bars indicate the standard deviation of the average. The backbone carbons were given the numbers −1, 0, +1, starting at the sn-3 position. The head group atoms were assigned the numbers −11 to −1 in the following order: the three terminal methyl C's, N, the two methylene C's, phosphate ester O, P, the two phosphate acid O's, and the phosphate ester O linking to the backbone. The atoms in the palmitoyl (—) and the oleoyl (···) tails were assigned positive numbers, beginning with the ester O's (1), the ester C's (2), and the carbonyl O's (3), and then continuing along the tails toward the terminal methyl groups, respectively.

refinement[51] which all indicate that the glycerol backbone is the most rigid portion of glycerophospholipid molecules in liquid-crystalline bilayers. The carbonyl and the phosphoric acid oxygens at positions +3 and −2, −3 in Figure 24, respectively, show increased mobility compared to neighboring atoms, which is to be expected for atoms participating in only one bond.

The flexibilities of the two tails are almost identical with the remarkable exception of the double bonded carbon atoms, positions 11 and 12 in Figure 24, which show an increased RMS value compared to the saturated sn-1 chain. In the following, we will refer to this increase as the "C=C-effect". The increased mobility of the double bonded carbons relative to the mobility of neighboring methylenes in the same tail is confirmed by experiment.[51] However, the explanation of the increase given by Wiener and White is based on the hypothesis that the hydrocarbon tails are tethered at both ends by the carbonyls and terminal methyls. This explanation must be objected because the hypothesis of tethered tail ends implies similar observations to be made for both tails. Our simulation data, which allow for direct comparison between the saturated and unsaturated tails, show clearly that the C=C-effect is due to the unsaturation because the increase in thermal mobility associated with the double bond is absent in the fully saturated chain (see Figure 24). Furthermore, the steady increase in thermal mobility toward the ends of the chains seen in our simulation is contradicting the idea of a tether restricting the motion of the terminal methyls.

From Figure 24 alone it is not clear whether the C=C-effect is a cooperative effect only present in aggregates of multiple lipids, or a geometric effect of the *cis*-bond which would then also be manifest in a simulation of a single lipid. An estimate of the necessary simulation time for a single lipid simulation can be obtained as follows: we were able to reproduce the C=C-effect whenever we used bilayer trajectories of 5 ps or longer for calculating average RMS values of lipid atoms. The C=C-effect did not appear if only a 1-ps trajectory was used. The effect was also absent if we used trajectories of more than 5 ps without averaging over all 200 lipids, i.e. if the RMS values (of a 46-ps trajectory) of a single lipid were plotted. This leads to an estimate of 200 × 5 ps = 10-ns simulation time necessary for a single lipid simulation to be statistically significant. We have performed such a 10-ns molecular dynamics simulation of one lipid in vacuum (unpublished results). In an analysis of the trajectory, we observed no distinctive increase in the RMS values of the double bonded carbons compared to the methylenes at the same position in the saturated tail. We, therefore, conclude that the C=C-effect is a cooperative phenomenon caused by the interactions of several lipids in a bilayer.

Final Structure. Ray traced images of the final structures of simulations I and II are presented in Figure 25. In both images the thin layer of restrained water (red) which prevents disintegration of the assemblies and assures their structural stability is visible. There is ample unrestrained water (orange) between the boundary and the lipids to ensure that the influence of the stochastic boundary on the lipids is small. The reduction in thickness of the bilayer after the gel to liquid-crystal phase transition is clearly visible. The most striking difference, perhaps, is the decrease in order of the hydrocarbon tails from the gel to the liquid-crystal phase. The difference in geometry of the water caps (ellipsoidal in simulation I and flat in simulation II) is a technicality and had no apparent influence on the structure and dynamics of the bilayer.

Discussion

In this paper we have presented the structure of a simulated patch of membrane of 200 lipid molecules with a size of 85 Å × 100 Å. This size is large enough to permit the addition of various biomolecules such as drugs, transmembrane proteins (e.g., bacteriorhodopsin,[4] porin,[92] or the photosynthetic reaction centers,[93,94] or proteins interacting with membranes (e.g., phospholipase A2 [95] or annexins[96]). The simulation included all atoms explicitly, except nonpolar hydrogen atoms, and described forces according to a conventional molecular dynamics force field. In order to account properly for transmembrane Coulomb interactions between head groups on opposite sides of the bilayer, long-range interactions were not cut-off. The volume simulated has been controlled by adjusting a stochastic boundary; this allowed control of the area per lipid, the quantity which determines the various phases of a membrane. Area per lipid values have been adjusted for two different membrane phases, the highly ordered gel phase and the less ordered liquid-crystal phase, the latter being assumed to constitute the native state of the membrane in biological cells. The computations for the respective molecular dynamics simulations consumed a total of 20 months of processor time on a machine of Cray 2 like processor power. This extraordinary effort was undertaken because it was expected that the membrane patch described will serve as a building block for numerous later investigations of the interactions of biopolymers with membranes, one of the most important issues in understanding the molecular biology of the cell (the membrane structure can be made available to other researchers as a pdb file by contacting the authors).

A first step toward studying heterogeneous membrane assemblies is to verify that the membrane model used does indeed show the properties of actual biological membranes. We have, therefore, presented in this paper evidence that the simulated membrane patch, in many respects, shows good agreement with observations. We employed for this purpose all properties that can be determined from molecular dynamics simulations lasting about 100 ps and for which data exist in the literature. Key characteristics determined are the deuterium order parameter profiles and RMS fluctuations along the lipid chains, the spatial distribution of lipid segments and water, the head group angles relative to the membrane normal, the pressure in the membrane, the lateral diffusion constant governing random motion over about 100 ps, and the repulsive steric protrusion pressure.[84] Close agreement with observations provides justification for the use of the membrane structure provided here for further studies of protein–membrane interactions. However, we certainly recognize and advocate the need for improvement of the membrane model provided here. The key shortcomings are the limitation in simulation time (a total of 263 ps thus far) and the relatively

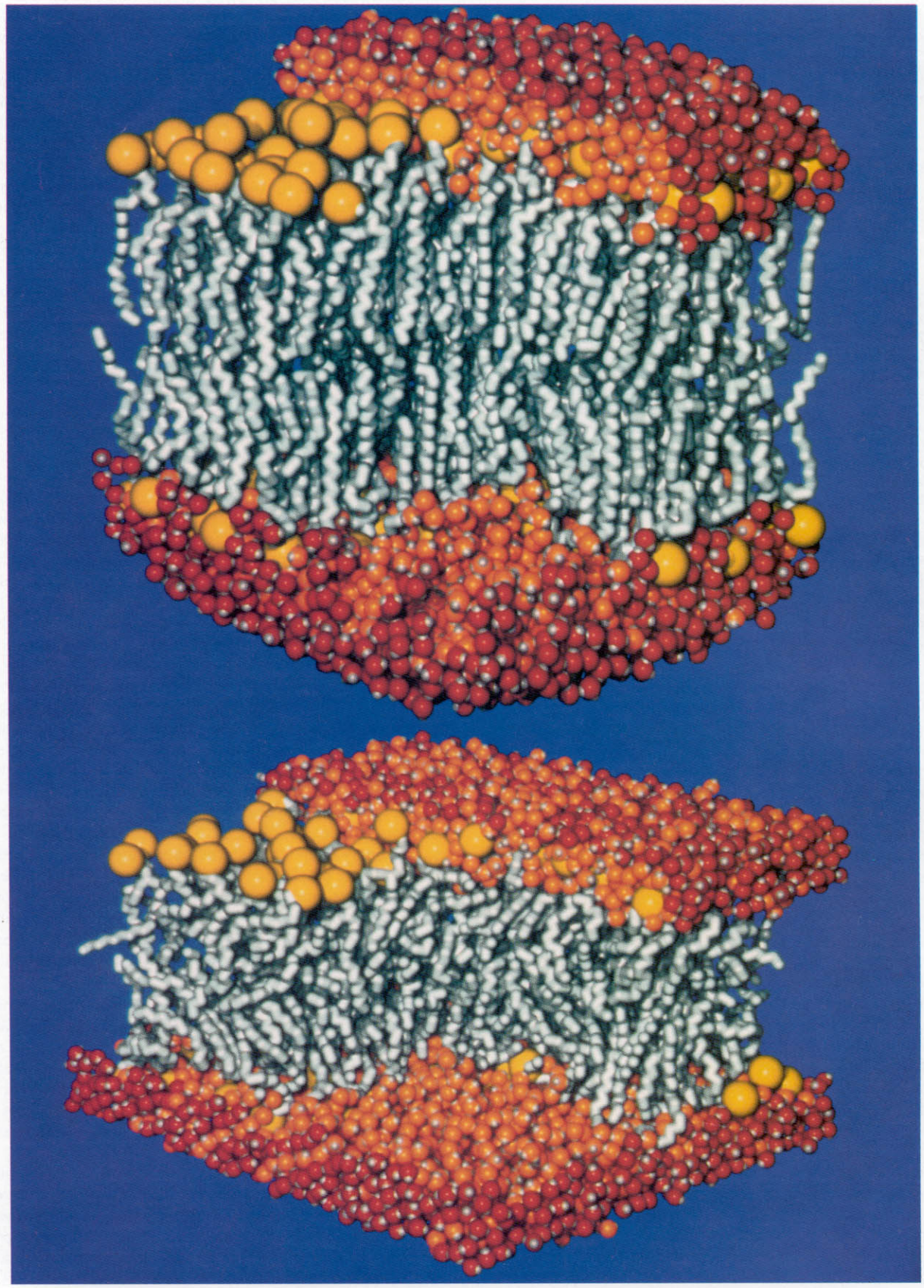

Figure 25. Final membrane structures resulting from simulation I (gel phase, top) and simulation II (liquid-crystal phase, bottom) of the POPC bilayer. A fraction of the water and the lipid molecules has been omitted to provide a view of the core of the membranes: (grey) hydrocarbon tails; (yellow spheres) head groups; (red) restrained water molecules; (orange) unrestrained water molecules.

small size of the membrane and the water layer, compared to biological cell dimensions. Improvements in these respects will yield better structures as well as better statistics for comparison with membrane data.

Most other simulations of membranes carried out so far dealt with smaller size systems or did not describe the system at the level of detail common to molecular dynamics methods, i.e., a level required to add biopolymers like drugs and proteins to describe the resulting interactions through molecular dynamics simulations. In the present simulations, as opposed to most previous simulations, we opted for use of a stochastic boundary rather than periodic boundary conditions because the stochastic boundary allows one to directly control the area per lipid molecule. The primary reason against the employment of periodic boundary conditions has been the difficulty of describing Coulomb interactions property for such systems. The importance of transmembrane Coulomb forces between head groups prevents the use of small cut-off ranges; on the other hand, suitable methods for carrying out Ewald summations for a planar lattice of very large (27 000 atoms) elementary cells are not currently available. However, we expect that once satisfactory structures of membrane patches in the various states of the membrane (i.e., gel, liquid crystal, etc.) exist, such structures can serve as building blocks for any array of patches treated as many identical copies in a plane.

There are many important aspects of membrane structure and dynamics other than the ones considered here, for example: the determination of rotational motions and of correlations in the motions of lipids; the hopping of lipids which should require minimal simulation times in the order of (area per head group)/(self-diffusion coefficient of lipids) $\approx$ 100 ns; the detailed description of tail dynamics such as the distribution of *trans*/gauche bonds and kinks; a demonstration of the existence of crankshaft motions in the tail; a test of anisotropies of the motion of lipid segments; the interdigitation of lipids at the hydrocarbon core; the determination of the surface potential of model membranes; the influence of applied electric fields, e.g., on the head group orientation; the tilt angle of lipid molecules; the possible occurrence of networks of hydrogen bonds in the head group region; an analysis of bond vibrations and a normal mode analysis of lipid vibrational motions in bilayers; radial distribution functions (hydration shells) of water around different lipid atoms; analysis of the property of the water layer near membranes; more extensive characterizations of the gel and liquid-crystal phases; and the comparison of membrane structures for different lipid compositions. Obviously, there exists an enormous research agenda for simulations of model membranes defined through many years of experimental work.

Therefore, we want finally to comment on the computational technology which will pave the way for molecular dynamics simulations of biological membranes. In this respect it is important to note that the present molecular dynamics study of the structure of lipid bilayers is probably the first instance of an investigation which required the technology of massively parallel computing. Much as the advent of supercomputers in the eighties opened an avenue for computational studies of biopolymers, the advent of massively parallel computers opens the possibility of computational investigations of molecular aggregates encompassing several tens of thousands of atoms. We have not emphasized in the present article the corresponding issues regarding the architecture of the parallel computer employed and the organization of computational and communication tasks across the computer since this had been described previously.[29,39-41]

The simulations reported here were carried out during the past 3 years on a 60 node computer designed and built in 1988 which achieved the same sustained performance during the molecular dynamics simulations as a Cray 2 processor. More recent models of parallel machines provide a speed increase of about a factor of 10 or more and improvements in node–node communication allow the cooperation of 10 times more processors. An efficient scheme for evaluation of Coulomb forces using a parallel implementation of the fast multipole algorithm (FMA[35,97-99]) should yield another factor of 10 in speed-up compared with the program presently used by us (in the reported simulations, we have employed the so-called distance class algorithm[1] which yields an acceleration by a factor of 10 compared to the straightforward summation over N^2 pairs). Hence, one can expect that within a year the simulations carried out by us over a time span of 20 months of uninterrupted computer time can be completed within a day. This perspective underscores that simulations of biological membranes and their integral proteins will soon be carried out routinely. The important role of membranes in biological cells will certainly provide a strong motivation for such studies. It is more difficult to predict in how far respective investigations will be impeded through lack of structural information of relevant proteins, but even given the present knowledge of protein structures (bacteriorhodopsin, the photosynthetic reaction centers, porin, phospholipase, annexins), exciting opportunities for future studies exist.

Acknowledgment. Participation of H.H. in the CECAM workshop "Molecular Dynamics Simulations of Proteins in Lipid Membranes" at the University of Paris at Orsay, Jan 1992, has contributed significantly to the perspectives set forth in this article. We thank Andreas Windemuth for stimulating discussions and rendering of Figure 25 and Barbara Napier for rendering of Figures 1 and 10 and help with other illustrations. This work was supported by the National Institute of Health Resource "Concurrent Biological Computing" under Grant no. 1 P41 RR05969*01. M.S. was partially supported by a NATO postdoctoral fellowship.

References and Notes

(1) Grubmüller, H.; Heller, H.; Windemuth, A.; Schulten, K. *Mol. Simul.* **1991**, *6*, 121.
(2) Büldt, G.; Gally, H. U.; Seelig, A.; Seelig, J.; Zaccai, G. *Nature* **1978**, *271*, 182.
(3) Pak, J. H.; Bork, V. P.; Norberg, R. E.; Creer, M. H.; Wolf, R. A.; Gross, R. W. *Biochemistry* **1987**, *26*, 4824.
(4) Henderson, R.; Baldwin, J.; Ceska, T.; Zemlin, F.; Beckmann, E.; Downing, K. *J. Mol. Biol.* **1990**, *213*, 899.
(5) König, S.; Pfeiffer, W.; Bayerl, T.; Richter, D.; Sackmann, E. *J. Phys. 2* **1992**, *2* (Aug), 1589.
(6) Marčelja, S. *Nature* **1973**, *241*, 451.
(7) Silver, B. L. *The Physical Chemistry of Membranes: An Introduction to the Structure and Dynamics of Biological Membranes*; Allen & Unwin and The Solomon Press, Publisher Creative Services Inc.: Jamaica, New York, 1985.
(8) Cevc, G.; Marsh, D. *Phospholipid Bilayers: Physical Principles and Models*; John Wiley & Sons: New York, 1987.
(9) Gennis, R. B. *Biomembranes: Molecular Structure and Function*; Springer-Verlag: New York, 1989.
(10) Pastor, R. W.; Venable, R. M.; Karplus, M. *Proc. Natl. Acad. Sci. USA* **1991**, *88*, 892.
(11) Schwyzer, R. *Biopolymers* **1991**, *31*, 785.
(12) McCammon, J. A.; Gelin, B. R.; Karplus, M. *Nature* **1977**, *267*, 585.
(13) Levitt, M. *J. Mol. Biol.* **1983**, *168*, 595.
(14) Karplus, M.; McCammon, J. A. *Annu. Rev. Biochem.* **1983**, *53*, 263.
(15) Brooks, C. L., III; Karplus, M.; Pettitt, B. M. *Proteins: A Theoretical Perspective of Dynamics, Structure and Thermodynamics*; John Wiley & Sons: New York, 1988.
(16) Edholm, O.; Johansson, J. *Eur. Biophys. J.* **1987**, *14*, 203.
(17) Levitt, M.; Sharon, R. *Proc. Natl. Acad. Sci. USA* **1988**, *85*, 7557.
(18) Warshel, A. Electrostatic free energy as the fundamental structure function correlator in proteins: Some perspectives from microscopic simulations of proteins functions. In *Modelling of Molecular Structures and Properties*; Rivail, J.-L., Ed.; Studies in Physical and Theoretical Chemistry, Vol. 71; Elsevier Science Publishers: Amsterdam, 1990; p 515.
(19) Michelangeli, F.; Grimes, E. A.; East, J. M.; Lee, A. G. *Biochemistry* **1991**, *30*, 342.
(20) Ploeg, P. v. d.; Berendsen, H. J. C. *J. Chem. Phys.* **1982**, *76*, 3271.
(21) Ploeg, P. v. d.; Berendsen, H. J. C. *Mol. Phys.* **1983**, *49*, 233.
(22) Damodaran, K. V.; Kenneth, M.; Merz, J.; Gaber, B. P. *Biochemistry* **1992**, *31*, 7656.
(23) Egberts, E.; Berendsen, H. J. C. *J. Chem. Phys.* **1988**, *89*, 3718.
(24) Watanabe, K.; Ferrario, M.; Klein, M. L. *J. Phys. Chem.* **1988**, *92*, 819.

(25) Wendoloski, J. J.; Kimatian, S. J.; Schutt, c. E.; Salemme, F. R. *Science* **1989**, *243*, 636.
(26) Pastor, R. W.; Venable, R. M.; Karplus, M. *J. Chem. Phys.* **1988**, *89*, 1112.
(27) Pastor, R. W.; Venable, R. M.; Karplus, M.; Szabo, A. *J. Chem. Phys.* **1988**, *89*, 1128.
(28) Loof, H. d.; Harvey, S. C.; Segrest, J. P.; Pastor, R. W. *Biochemistry* **1991**, *30*, 2099.
(29) Heller, H.; Grubmüller, H.; Schulten, K. *Mol. Simul.* **1990**, *5*, 133.
(30) Windemuth, A.; Schulten, K. *Mol. Simul.* **1991**, *5*, 353.
(31) Beeman, D. *J. Comput. Phys.* **1976**, *20*, 130.
(32) Streett, W. B.; Tildesley, D. J.; Saville, G. *Mol. Phys.* **1978**, *35*, 639.
(33) Greengard, L.; Rohklin, V. *J. Comput. Phys.* **1987**, *73*, 325.
(34) Board, J. A., Jr.; Batchelor, R. R.; Leathrum, J. F., Jr. High performance implementations of the fast multipole algorithm. *Symposium on Parallel and Vector Computation in Heat Transfer, Proceedings of the 1990 AIAA/ASME Thermophysics and Heat Transfer Conference*; American Society of Mechanical Engineers: New York, 1990.
(35) Board, J. A., Jr.; Causey, J. W.; Leathrum, J. F., Jr.; Windemuth, A.; Schulten, K. *Chem. Phys. Lett.* **1992**, *198*, 89.
(36) Wiener, M. C.; White, S. H. *Biophys. J.* **1991**, *59*, 162.
(37) Lafleur, M.; Cullis, P. R.; Bloom, M. *Eur. Biophys. J.* **1990**, *19*, 55.
(38) Nagle, J. F.; Wiener, M. C. *Biochim. Biophys. Acta* **1988**, *942*, 1.
(39) Boehncke, K.; Heller, H.; Grubmüller, H.; Schulten, K. Molecular dynamics simulations on a systolic ring of transputers. In *NATUG 3: Transputer Research and Applications 3*; Wagner, A. S., Ed.; North American Transputer Users Group, IOS Press: Amsterdam, 1990; p 83.
(40) Heller, H.; Schulten, K. *Chem. Des. Autom. News* (*CDA News*) **1992**, *7* (Aug), 11. Also published in: *Proceedings of the Fifth Conference on Neural Networks and Distributed Parallel Processing*; Sayegh, Samir I., Ed.; Indiana University—Purdue University at Fort Wayne: Fort Wayne, IN, in press. (Also published as: Beckman Institute Technical Report TB-92-09.)
(41) Sinha, A.; Heller, H.; Schulten, K. *Comput. Phys. Commun.* **1992**, in press (Beckman Institute Technical Report TB-92-13).
(42) Heller, H. Dynamiksimulation sehr grosser Makromoleküle am Beispiel des photosynthetischen Reaktionszentrums von Rhodopseudomonas viridis. Diploma thesis, Physics Department, Technical University of Munich, Garching/Munich, 1988.
(43) Banko, B.; Heller, H. *User Manual for EGO*; Beckman Institute Technical Report UIUC-BI-TB-92-07; Theoretical Biophysics Group at the University of Illinois at Urbana-Champaign, Physics Department, Beckman Institute; Urbana, IL, 1991.
(44) Brooks, B. R.; Bruccoleri, R. E.; Olafson, B. D.; States, D. J.; Swaminathan, S.; Karplus, M. *J. Comput. Chem.* **1983**, *4*, 187.
(45) Brünger, A. T. *X-PLOR*; The Howard Hughes Medical Institute and Department of Molecular Biophysics and Biochemistry, Yale University: New Haven, CT, May 1988.
(46) Brünger, A. T. *X-PLOR, Version 2.1*; The Howard Hughes Medical Institute and Department of Molecular Biophysics and Biochemistry, Yale University: New Haven, CT, 1990.
(47) Verlet, L. *Phys. Rev.* **1967**, *159* (Jul), 98.
(48) Ryckaert, J.-P.; Ciccotti, G.; Berendsen, H. J. C. *J. Comput. Phys.* **1977**, *23*, 327.
(49) Raine, A. R. C. Molecular dynamics simulation of proteins on an array of transputers. In *Applications of Transputers 2., Proceedings of the Second International Conference on Applications of Transputers*, Pritchard, D. J., Scott, C. J., Eds.; IOS Press: Amsterdam, Netherlands, 1990; p 272.
(50) *Quanta*; Polygen Corp.: Waltham, MA, 1988.
(51) Wiener, M. C.; White, S. H. *Biophys. J.* **1992**, *61*, 434.
(52) Jorgensen, W. L.; Chandrasekhar, J.; Madura, J. D.; Impey, R. W.; Klein, M. L. *J. Chem. Phys.* **1983**, *79*, 926.
(53) Schlenkrich, M.; MacKerell, A. D., Jr.; Karplus, M. Manuscript in preparation.
(54) Berkowitz, M.; McCammon, J. A. *Chem. Phys. Lett.* **1982**, *90*, 215.
(55) Brooks, C. L., III; Brünger, A.; Karplus, M. *Biopolymers* **1985**, *24*, 843.
(56) Brünger, A. T.; Brooks, C. L., III; Karplus, M. *Chem. Phys. Lett.* **1984**, *105*, 495.
(57) Berendsen, H. J. C.; Postma, J. P. M.; Gunsteren, W. F. v.; DiNola, A.; Haak, J. R. *J. Chem. Phys.* **1984**, *81*, 3684.
(58) Lide, D. R., Ed. *CRC Handbook of Chemistry and Physics*, 73 ed.; CRC Press, Inc.: Boca Raton, FL, 1992.
(59) Beveridge, D. L.; DiCapua, F. M. *Annu. Rev. Biophys. Biophys. Chem.* **1989**, *18*, 431.
(60) Seelig, J.; Waespe-Šarčevič, N. *Biochemistry* **1978**, *17*, 3310.
(61) Nadler, W.; Tavan, P.; Schulten, K. *Eur. Biophys. J.* **1985**, *12*, 25.
(62) Berendsen, H. J. C.; Gunsteren, W. F. v. Practical algorithms for dynamic simulations. In *Proceedings of the International School of Physics, "Enrico Fermi"*, Vol. on course 97; Ciccotti, G. C., Hoover, W. G., Eds.; North-Holland: Amsterdam, 1986; p 43.
(63) König, S. Private communication, 1993.
(64) Seelig, A.; Seelig, J. *Biochemistry* **1977**, *16*, 45.
(65) Seelig, J.; Seelig, A. *Q. Rev. Biophys.* **1980**, *13*, 19.
(66) Seelig, J. *Q. Rev. Biophys.* **1977**, *10*, 353.
(67) Galla, H.-J.; Hartmann, W.; Theilen, U.; Sackmann, E. *J. Membr. Biol.* **1979**, *48*, 215.
(68) Pfeiffer, W.; Henkel, T.; Sackmann, E.; Knoll, W.; Richter, D. *Europhys. Lett.* **1989**, *8*, 201.
(69) Cohen, M. H.; Turnbull, D. *J. Chem. Phys.* **1959**, *31*, 1164.
(70) Rand, R. P.; Parsegian, V. A. *Biochim. Biophys. Acta* **1989**, *988*, 351.
(71) Wiener, M. C.; White, S. H. *Biophys. J.* **1992**, *61*, 428.
(72) Seelig, A.; Seelig, J. *Biochemistry* **1974**, *13*, 4839.
(73) Schindler, H.; Seelig, J. *Biochemistry* **1975**, *14*, 2283.
(74) Seelig, J.; Browning, J. L. *FEBS Lett.* **1978**, *92*, 41.
(75) Seelig, J.; Macdonald, P. M.; Scherer, P. G. *Biochemistry* **1987**, *26*, 7534.
(76) Pearson, R. H.; Pascher, I. *Nature* **1979**, *281*, 499.
(77) Akutsu, H.; Nagamori, T. *Biochemistry* **1991**, *30*, 4510.
(78) Büldt, G.; Gally, H. U.; Seelig, J.; Zaccai, G. *J. Mol. Biol.* **1979**, *134*, 673.
(79) Owenson, B.; Pratt, L. R. *J. Phys. Chem.* **1984**, *88*, 6048.
(80) Northrup, S. H.; Curvin, M. S. *J. Phys. Chem.* **1985**, *89*, 4707.
(81) Egger, M.; Ohnesorge, F.; Weisenhorn, A. L.; Heyn, S. P.; Drake, B.; Prater, C. B.; Gould, S. A. C.; Hansma, P. K.; Gaub, H. E. *J. Struct. Biol.* **1990**, *103*, 89.
(82) Marčelja, S.; Radic, N. *Chem. Phys. Lett.* **1976**, *42*, 129.
(83) Israelachvili, J. N.; Wennerström, H. *Langmuir* **1990**, *6*, 873.
(84) Israelachvili, J. N.; Wennerström, H. *J. Phys. Chem.* **1992**, *96*, 520.
(85) McIntosh, T. J.; Simon, S. A. *Biochemistry* **1986**, *25*, 4058.
(86) McIntosh, T. J.; Magid, A. D.; Simon, S. A. *Biochemistry* **1989**, *28*, 7904.
(87) Radmacher, M.; Tillmann, R. W.; Fritz, M.; Gaub, H. E. *Science* **1992**, *257*, 1900.
(88) Hitchcock, P. B.; Mason, R.; Thomas, K. M.; Shipley, G. G. *Proc. Natl. Acad. Sci. USA* **1974**, *71*, 3036.
(89) Elder, M.; Hitchcock, P.; Mason, R.; Shipley, G. G. *Proc. R. Soc. London A.* (*Math. Phys. Sci.*) **1977**, *354*, 157.
(90) Strenk, M. L.; Westerman, P. W.; Doane, J. W. *Biophys. J.* **1985**, *48*, 765.
(91) Braach-Maksvytis, V. L. B.; Cornell, B. A. *Biophys. J.* **1988**, *53*, 839.
(92) Garavito, R. M.; Jenkins, J.; Jansonius, J. N.; Karlson, R.; Rosenbusch, J. P. *J. Mol. Biol.* **1983**, *164*, 313.
(93) Deisenhofer, J.; Michel, H. The photosynthetic bacterial reaction center: Structure and dynamics. *In The crystal structure of the photosynthetic reaction center from Rhodopseudomonas viridis*; Breton, J., Verméglio, A., Eds.; NATO ASI Series A: Life Sciences, Vol. 149; Plenum Press: London, 1987; p 1.
(94) Michel, H.; Deisenhofer, J. *Chem. Scr.* **1987**, *27B*, 173.
(95) Dijkstra, B. W.; Kalk, K. H.; Hol, W. J. H.; Drenth, J. *J. Mol. Biol.* **1983**, *147*, 97.
(96) Creutz, C. E. *Science* **1992**, *258*, 924.
(97) Greengard, L.; Gropp, W. D. A parallel version of the fast multipole method. Technical report, Rept. YALEU/DCS/RR-640, 1988.
(98) Board, J. A., Jr.; Leathrum, J. F., Jr. The fast multipole algorithm on transputer networks. In *Transputer Research and Applications 3, NATUG-3* Proceedings, Wagner, A. S., Ed.; The North American Transputer Users Group, IOS Press: Amsterdam, 1990; p 63.
(99) Leathrum, J. F., Jr.; Board, J. A., Jr. Parallelization of the fast multipole algorithm using the B012 transputer network. In *TRANSPUTING91*; Stiles, D., Kunii, T. L., Bakkers, A., Eds.; 10S Press: Amsterdam, The Netherlands, 1991; Vol. 1, p 296.